

Anonymous Referee #1

Received and published: 28 June 2016

This paper describes a range of different set-ups for a high resolution atmospheric model simulating polynyas in the Laptev Sea. The set-up involves the use of “tiles” which are sub-grid scale parametrization of thin sea ice. The quality of the model appears fine, and the number of simulations are impressive. Citations given are generally fine, and the technical quality of the figures are OK. Polynyas are important regions with substantial ice production and very high heat fluxes, and are thus an important part of the Cryosphere.

With the above in place one would expect that the paper would be in fairly good shape, but I am sorry to state that this is not the case.

R#1: The attention to detail is totally overwhelming, and there is almost nothing learned in terms of physics.

A: We agree that many details of the results were included in the manuscript, which could make it difficult to focus on the main aspects. The primary objective of the paper was to assess the sensitivity of ice production of Laptev Sea polynyas on the chosen assumption for thin-ice thickness of a tile approach for subgrid-scale energy fluxes. This is not a specific problem of the used model (CCLM), but a general problem of all regional climate models using the tile approach. To our knowledge, it is generally assumed that the subgrid fraction not covered by sea ice is assumed to be open water (e.g. in the recently published ASR data set). We could show that the ice production is very sensitive to the tile-approach and thin-ice thickness, which affects also the atmospheric boundary layer structure. However, we agree that for example the latter issue was not discussed sufficiently.

Changes in the manuscript: In the revised manuscript we change the structure of the paper and focus more on the physical aspects by simultaneously reducing the details of the results, i.e. we present only the results of three simulations and show sensitivities only where useful. We further changed the title to: “Quantification of ice production in Laptev Sea polynyas and its sensitivity to thin-ice parameterizations in a regional climate model” to better reflect to content of the manuscript.

R#1: The use of abbreviations also has no end, and is a clear sign that at this level the text is more like a data report intended for those that may apply the same model system in a future study. One look at Table 3 should say it all.

A: Multi-model or sensitivity studies always include a lot of abbreviations. We accept this remark and thus reduce the amount of details and abbreviations to a necessary minimum.

Changes in the manuscript: The abbreviations of the simulation runs will be homogenized and we will change the structure of the manuscript so that it focuses on the scientific aspects not on the technical details. Therefore, we restrict the presented results to three simulations: C05nt (the reference), C05wt0 (subgrid-scale open-water scenario) and C05-50/1 (most realistic assumptions). We will change these abbreviations to: C05-ref, C05-10/0, and C05-50/1. Table 3 will be condensed.

R#1: For the main conclusion not much has been learned about the atmospheric boundary layer, where the model actually should resolve processes in a better way than earlier model attempts. That the overall heat loss increases along with the total ice production when areas of thinner ice is added as a new lower

boundary condition is indeed what is expected and does not contribute to an increased scientific understanding.

A: We agree that we did could include more results on the ABL. However, we have already addressed some important aspects (impact on the warm plume formation, turbulence structure, cloud formation), which contribute to an increased quantitative understanding of the processes and their feedbacks.

Changes to the manuscript: We will rewrite the ABL part to point out the main conclusions.

R#1: The text is also written only from a modellers perspective, without even the most basic understanding of processes in a polynya in nature. Moving downwind from the beach there is CONTINUOUS change from open water to thicker and thicker sea ice, much like the MODIS observations plotted in Figure 13. In essence resolving the heat fluxes and the ice thickness inside a polynya is a coupled problem. Such coupling has been done albeit in a very simple way starting with Pease (1987). I'm not saying that you should invent a new downwind thickness parametrization for thickness, but rather state that you have made your choices, and then how this is simplified from nature.

A: We see the point that the text is focused too much on the modeller's perspective, however it is not clear to us how we missed "the most basic understanding" of polynya processes. We did not intent to give a too detailed introduction on polynya processes and thus cited relevant papers for more information. But we agree that some more information on e.g. polynya formation and the spatial structure of thin-ice within a polynya are useful additions. We are aware that the ice thickness increases with downwind direction, which is not represented in CCLM yet. Figure 13 shows the spatio-temporal histogram of thin-ice within Laptev Sea polynyas retrieved from MODIS data, which is not to confuse with the spatial sequence of thin-ice in a polynya. Our implementations to CCLM are just the first step to represent fractional sea ice, which was not present in all CCLM simulations before. In this context, we would like to note that even Polar-WRF does not use spatial distributions of thin-ice within polynyas, in fact in WRF there is always subgrid-scale open-water assumed, which is much more unrealistic then our assumptions. Comparing e.g. Fig.11a and Fig.11c there is still a downwind structure of the ice production visible for the WNS polynya (opened on 30 April 2008), which is not present in the reference simulation (Fig.11a) (and weaker for the other simulation runs).

Changes in the manuscript: We will comment on our chosen assumptions on the thin-ice distribution and that it is a simplification to the thin-ice structure observed in nature. This is an important point we missed to mention in the manuscript.

R#1: A statement like "open water areas particularly produce new ice and are hence rarely free of ice" (Page 6, line 10) is not correct at all. Polynyas stay open for many hours during strong wind events that effectively transport sea ice (frazil, grease, pancake, solid ice) downwind (Morales-Maqueda et al 2004, Fig. 17). An open polynya length along the wind direction between 10 – 30 km is not uncommon.

A: We guess our formulation might be too imprecise as we actually meant that the heat loss is highest over open-water areas. These open-water areas quickly produce frazil and grease ice, which is then advected downstream and consolidates to thicker ice, hence the continuous increase in thickness mentioned in the previous comment. However, based on field experience of the authors we argue that the fraction of the Laptev polynya area that is completely free of ice is

relatively small during winter (as illustrated in the appendix and Fig.13 of our paper).

Changes in the manuscript: We will reformulate this sentence to make clear what we wanted to express and we further add the information that in our simulations it is assumed that new ice is instantly advected downstream so that the initial thin-ice thickness is restored after every time step. We will also add the word „wintertime“ to the polynyas.

R#1: The most interesting part of this study is the response of the atmospheric boundary layer, as shown in Figure 7. But here two plots should be shown, the “best” case and the similar without the tiles (C05nt – perhaps, it is just a total misuse of abbreviations here). This should be the case also for Figure 5, Figure 6, and Figure 11. All the tables should only compare values between your “best” model simulation and the one without the tiles. The details are not interesting, unless you have some way of evaluating the model performance.

A: We think that the most interesting part is the ice production, since this has impacts also for the ocean circulation. We will pick up the suggestion of taking the “best” model simulation as reference.

Changes in the manuscript: As mentioned above we will restrict the presentation of results to three simulation runs. That is we reduce the amount of subplots of the mentioned figures and also reduce the tables to a necessary minimum.

R#1: The paper needs to be totally rewritten if it is to be published as a scientific article. First – make your choice on the “best” model simulations, and present all relevant results to this one case first. Then compare to existing simulations without the tiles. At the end you can include some sensitivities to some of the different choices made, like the different thin ice thickness’ inside the polynya. This reviewer has not been convinced that new scientific understanding has been achieved here, but I’m willing to review a new version of a totally rewritten paper if that is submitted.

Sorry to be so negative, but this version can be saved as a technical report for researchers

that will work on the same model in the future. No one else would have the interest to read about all these details, and you have not done the important scientific job it is to extract the new understanding based on your model simulations.

A: We have a different opinion concerning the reviewer’s statements about scientific understanding and technical report, but we will restructure and rewrite the manuscript also considering the remarks of reviewer #2 (who states that we show the significant results).

Changes in the manuscript: As mentioned above we will present and compare the results of three simulation runs: a reference without the tile-approach, one run with subgrid-scale open-water as a possible upper limit, and one run which we think is the most realistic configuration.

Appendix

Ice-free polynyas in the Laptev Sea

In wintertime, only a very small percentage of a polynya is ice-free, as it was shown by many studies and is illustrated by the following two figures from satellite data and airborne in-situ observations (from Willmes et al. 2010).

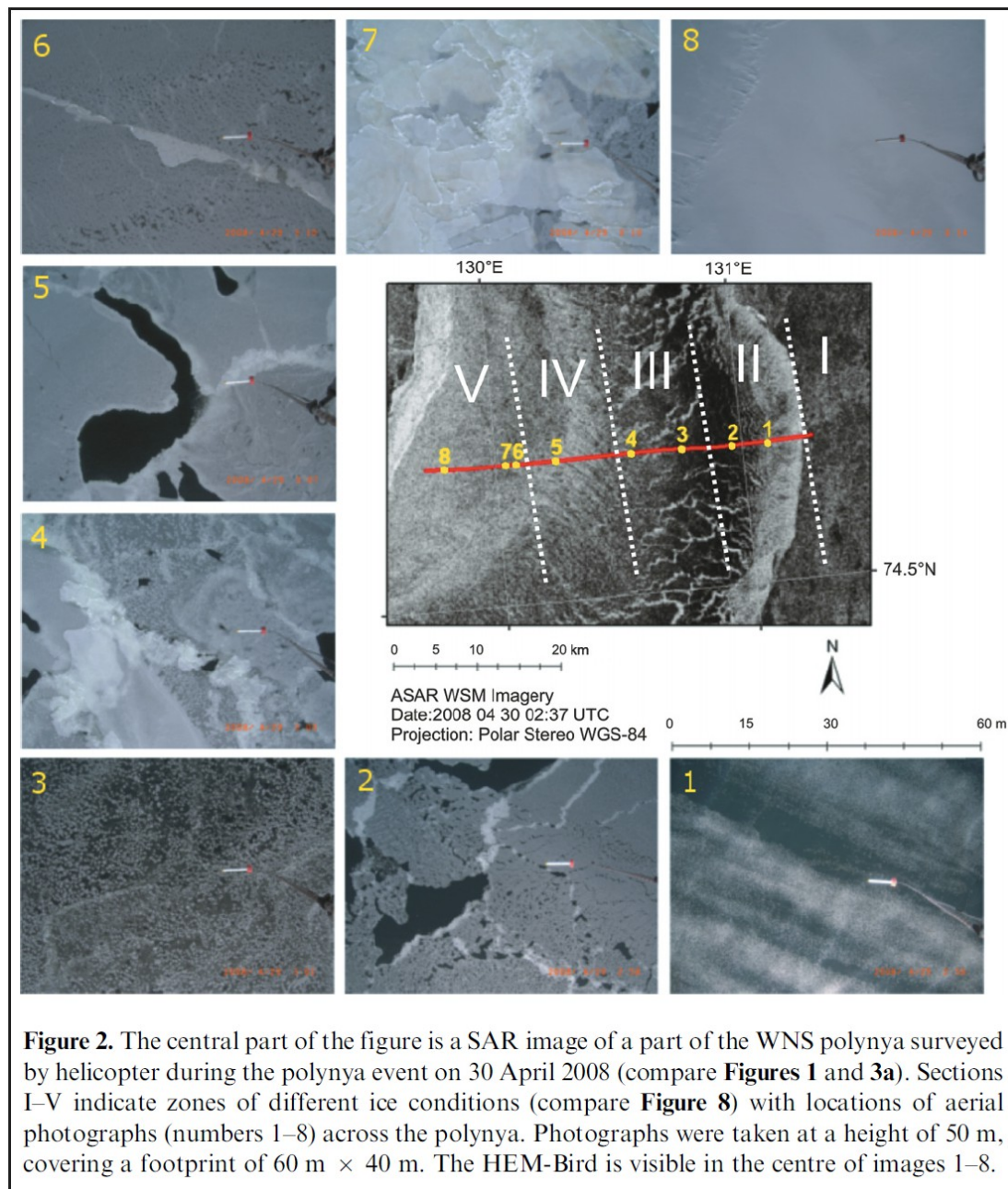


Figure 2. The central part of the figure is a SAR image of a part of the WNS polynya surveyed by helicopter during the polynya event on 30 April 2008 (compare **Figures 1** and **3a**). Sections I–V indicate zones of different ice conditions (compare **Figure 8**) with locations of aerial photographs (numbers 1–8) across the polynya. Photographs were taken at a height of 50 m, covering a footprint of 60 m × 40 m. The HEM-Bird is visible in the centre of images 1–8.

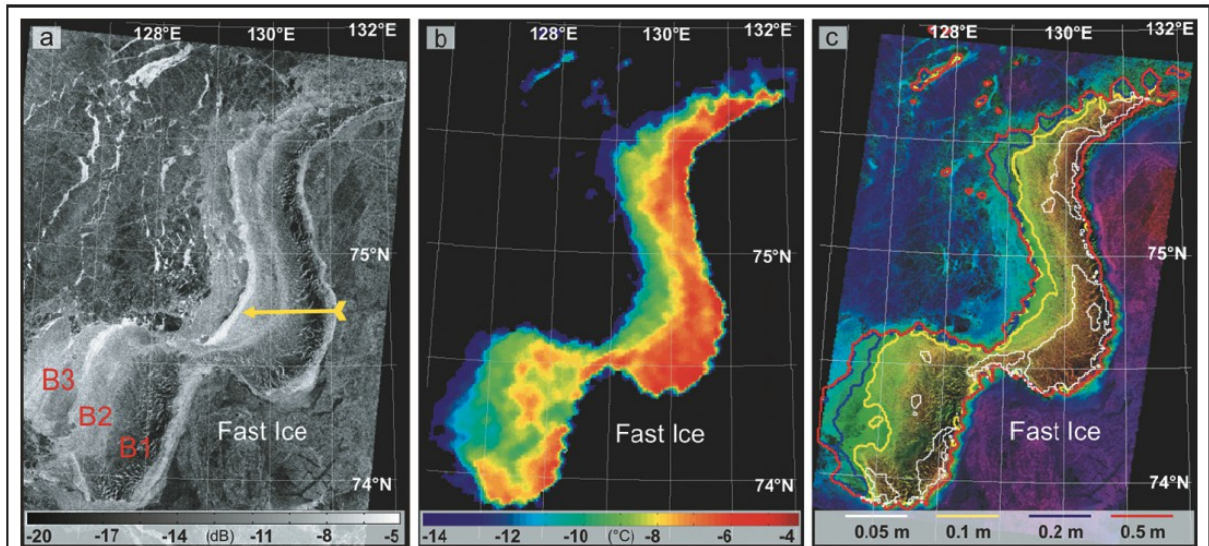


Figure 3. Western New Siberian polynya. (a) Envisat SAR backscatter for 30 April 2008 at 0237 UTC. Characteristic backscatter bands B1–B3 and the helicopter flight track at 0225 UTC are indicated. (b) Surface temperature (between $-14\text{ }^{\circ}\text{C}$ and $-4\text{ }^{\circ}\text{C}$) as derived from AVHRR IR brightness temperatures from 29 April 2008 at 2000 UTC. (c) Composite of (a) and (b) together with contour lines (0.05, 0.1, 0.2, and 0.5 m) of the thermal ice thickness hi_{TH} (derived from data in (b)).

An additional example is shown by Adams et al. (2013):

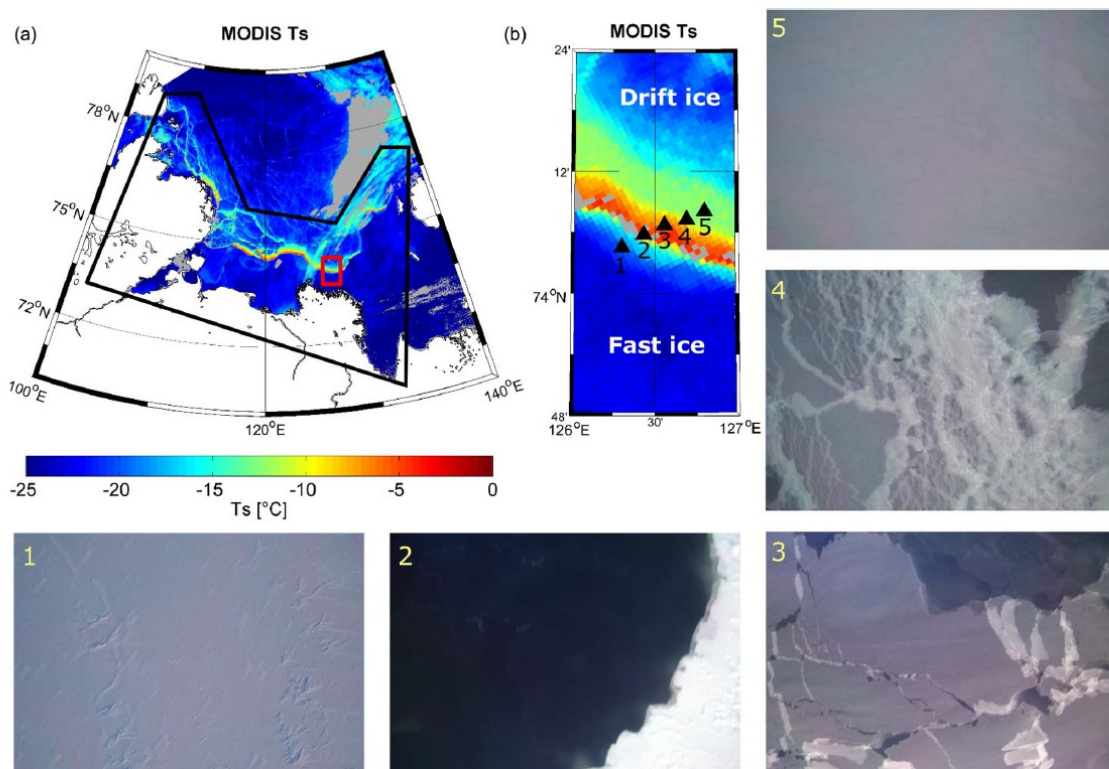


Fig. 1. (a) Map of MODIS (MOD29) ice-surface temperatures in the Laptev Sea on 26 March 2009 1220 UTC. The black line broadly indicates the polynya region in the Laptev Sea. The mask is based on [37]. The small rectangle in (a) locates the subset shown in (b). The north-east oriented stripes around $-15\text{ }^{\circ}\text{C}$ located at $120^{\circ}\text{--}140^{\circ}\text{ E}$ and $75^{\circ}\text{--}78^{\circ}\text{ N}$ are clouds not identified by the MODIS cloud mask. (b) Subset of the Laptev Sea. Triangles in the map denote the positions of five aerial photographs which were taken on 26 March 2009 0800 UTC during the TRANSDRIFT XV expedition. Black pixels (shown in gray in color version of this figure) in map (a) and (b) mark data gaps due to clouds.

Anonymous Referee #2

Received and published: 1 July 2016

General comments:

The authors implement a tile-approach into the atmospheric COSMO-CLM model to account for subgrid-scale sea-ice inhomogeneities and examine the impact on estimated sea ice production in the Laptev Sea polynyas. Due to huge differences between sea-ice and open water properties and the linear dependency of energy fluxes on these properties, the implementation of the tile-approach is a significant improvement of the COSMO-CLM model. The configuration of the simulations is complex: 182 daily simulations for each setup with initial conditions based on AMRS-E sea ice concentration, PIOMAS sea ice thickness, and MODIS based assumption for polynya sea-ice thickness and sub-grid scale ice thickness. Overall the setup is convincing and promises to give the most realistic results for ice production given the limitations of the very simple sea ice module in COSMO-CLM. In addition to the main finding that the ice production can increase by a factor of 2, the authors discuss a number factors documenting how difficult it is to accurately determine ice production in polynyas.

In spite of the quality of the simulations and the significance of the results major revisions are required.

R#2: My main concern is that the current manuscript fails to appeal to scientists who are not familiar with polynya processes in the Laptev Sea and/or are not using the COSMO-CLM model. Required background information and motivation (e.g. formation of polynyas, importance of polynya ice production) are missing in the study.

A: Although we mentioned some aspects of polynya formation in the Laptev Sea, we agree that too few information is given for readers which are not familiar with polynyas and how they are implemented in regional climate models besides CCLM.

Changes in the manuscript: We will add more information and details on the polynya processes in the Laptev Sea and how polynyas are represented in RCMs. Further we will state more clearly the objectives of our study.

R#2: The discussion of the results is too restricted to differences with one remote sensing product (Willmes et al., 2011) and potential adjustments of the COSMO-CLM model. What can somebody learn from this study who is not using COSMO-CLM? Prescribing the subgrid-scale ice thickness cannot be the best solution to simulate polynya processes. What are consequence from your study for applying a more complex sea ice model which aims to simulate the processes?

A: We chose to compare our results to the estimates of Willmes et al. (2011) because it is based on the same polynya masks and the same satellite date (i.e. on the same original AMSR-E product). We think with the product of Willmes et al. (2011) we chose the most suited product available for our comparison, as mentioned in the manuscript. Otherwise, even more issues arise for comparisons with model results.

We think that the results of the sensitivity study are valuable also for other models using the tile approach and prescribed sea ice coverage. Although we use a rather simple approach to represent subgrid-scale ice thickness, some of the issues remain even if more complex approaches are used. Subgrid open water or thin ice fraction is also a problem for complex sea-ice/ocean models.

Changes in the manuscript: We will adapt the discussion section by commenting on the general relevance of our results for other RCMs and consequences if more complex sea ice models are used within an RCM. As far as the remote sensing

product is concerned, we already tried to generalize from our results, so we do not see the requirement to adapt the paragraphs dealing with this issue.

R#2: Specific comments:

1. Abstract: too long; too many details about setup; mention that COSMO-CLM is atmospheric model; not clear whether numbers are winter averages or extremes from case studies. Better give numbers from preferred reference run. Last sentence too specific for COSMO-CLM setup (see General Comments.)

A: We agree on the issues raised by the reviewer.

Changes in the manuscript: The abstract will be revised and shortened considerably. We will also make clear what the numbers represent.

2. Introduction: mainly just technical introduction; paragraph about polynyas and their importance missing; mention discrepancy of estimates of polynya ice production from previous studies.

A: We put the paragraph on polynyas within section 2 as 2.1. This was not the best option and the introduction (but also the general structure of the manuscript) needs to be overdone.

Changes in the manuscript: We will move and integrate section 2.1 to the introduction and add more background information on polynyas, their importance and what was not represented in previous studies.

3. Configuration of CCLM / initial conditions: If a model grid point has e.g. SIC = 60%, is this grid box regarded as polynya box in which 60% of the area is covered by ice with a thickness of TIT (10 cm for model run C05wt1) and 40% with a thickness of the subgrid-scale TIT (1cm for this model run)? Do the ice thickness, TIT and subgrid-scale TIT change during the 24h simulation period?

A: This is correct, the SIC of AMSRE constitutes the grid-scale ice thickness (10cm) in this example and 1-SIC is the 'open-water' fraction or the area with subgrid-scale ice thickness. However, this differentiation is not restricted to polynyas but is applied generally for fractional sea ice. The ice thickness is allowed to change within a time step, but is restored after every time step.

Changes in the manuscript: We will reformulate the sentences concerning these two issues to make the procedure more clearly.

4. Page 8, line 13: "the turbulent exchange coefficient CH is variable in time":

Why? Please write "is a function of ..."

Changes in the manuscript: We will reformulate the sentence.

5. Verification with in situ data: The AWS were deployed over the fast ice and Table 3 and Figure 4 document that there are no significant differences between the sensitivity runs as long SIC > 95 %. Just show results from one simulation (C05nt) in Table 3. Figure 4 could be omitted in my opinion.

A: We agree on this comment.

Changes in the manuscript: We will remove Fig.4 from the manuscript and restrict Tab. 3 to three simulations (C05nt, C05wt0, and C05-50/1). We will also change the abbreviations of the simulation runs to: C05, C05-10/1, C05-50/1 for a better readability.

6. Case study on 4 January 2008: The differences in Figure 5 and 6 are quite difficult to spot and at this stage the reader is not aware whether you have a preferred reference run. Might be helpful to change order and to focus just on the preferred run for the case study

A: We agree on this comment.

Changes in the manuscript: We will restrict Fig.5 and Fig.6 to only three simulation runs (see comment before). Further we will introduce in the beginning of section 2, what configuration is the reference and what is the optimal one in our opinion so that the reader can follow our chain of arguments more easily.

7. Conclusions: Only present numbers from your preferred reference run. Put your results in wider context. See general comment. Add a paragraph about how your

results might help to simulate polynya processes using a more complex sea ice model including recent advances of frazil ice modules (e.g. Wilchinsky et al., JPO 2015).

A: We agree on this comment.

Changes in the manuscript: We will extend the conclusion section by mentioning what our results mean for more complex sea ice models and restrict the presentation of numbers to our preferred simulation.

8. Give numbers with adequate decimals in text and tables (e.g. +110% instead of 109.7% in line 11 or 29 km³ instead of 29.05 km³ in line 14).

Changes in the manuscript: We will change the numbers accordingly to improve the readability of the manuscript.

Sensitivity Quantification of ice production estimates in Laptev Sea polynyas and its sensitivity to the parameterization of subgrid-scale sea-ice inhomogeneities thin-ice parameterizations in COSMO-CLM regional climate model

Oliver Gutjahr¹, Günther Heinemann¹, Andreas Preußner¹, Sascha Willmes¹, and Clemens Drüe¹

¹Department of Environmental Meteorology, University of Trier, Behringstraße 21, 54296 Trier, Germany

Correspondence to: Oliver Gutjahr (gutjahr@uni-trier.de)

Abstract. ~~A tile-approach (TA) for the calculation of~~ The quantification of sea-ice production in the Laptev Sea polynyas is important for the dense water formation of the global thermohaline circulation and the energy balance over fractional sea ice was implemented into the standard version of the COSMO-CLM (CCLM) model. The tile-approach accounts for subgrid-scale energy exchange within polynyas and leads, which are neglected in the CCLM standard version. We perform six simulations for the area of the Laptev Sea at a horizontal resolution of 5 km heat exchange with the atmosphere. We estimated the ice production for the winter season 2007/08 (Nov.-Apr.) with different grid-scale and subgrid-scale ice thicknesses within polynyas based on simulations with the regional climate model COSMO-CLM (CCLM) at a horizontal resolution of 5 km and compared it to remote sensing estimates. A reference run without TA assumes a grid-scale ice thickness of 10 cm within polynyas (derived as the mean thin-ice thickness in the Laptev polynyas from satellite data). Three sensitivity runs were performed for 10 cm grid-scale ice thickness and subgrid-scale open water, thin-ice of 1 cm, and 10 cm thickness. Two runs use a and five sensitivity simulations were performed with different assumptions on grid-scale ice thickness of 50 cm and a and subgrid-scale ice thickness of 5 cm and 1 cm, respectively. We analyse the sensitivity of the ice production (IP) in this winter and compare them with estimations from remote sensing methods considered within polynyas, using a tile approach (TA) for fractional sea ice. In addition, the impact of the surface heat exchange on the atmospheric boundary layer (ABL) is shown for a case study was investigated.

~~The use of the TA causes an increased heat loss over polynyas, which is up to +109.7% higher in. About 29.1 km³ of ice production were estimated for the reference simulation which varies by up to +124% in dependence on the thin-ice assumptions. For realistic assumption the IP increases by +39%. The use of the TA enlarges the area and enhances the magnitude of the sensitivity runs compared to the reference run. This enhanced heat loss is caused by an increase of the surface temperatures and the near-surface wind speed within and above polynyas. The surface temperatures are +6°C to +16°C higher than in the reference simulation. The reference ice production of 29.05 km³ increases due to the heat loss from polynyas up to +110% if subgrid-scale open water is assumed, and by +20% for realistic assumptions. This enhanced heat loss in causes in turn higher ice production rates and stronger impact on the ABL structure over the polynyas. The study shows that IP is highly sensitive to the sensitivity simulations by +0.3% to +124.5%. The comparison of the IP with estimates from~~

remote sensing methods remains difficult due to different assumptions on the combination with atmospheric data, turbulent transfer coefficients for heat and polynya definitions.

In summary, the consideration of subgrid-scale energy fluxes in form of the tile approach yields a more realistic representation of thin-ice parameterizations for fractional sea ice cover. However, the impact on IP and the ABL depends strongly on the choice of the subgrid-scale ice thickness, which should be consistent with satellite-derived ice thickness distribution in polynyas. Increased ice production in the Laptev Sea would have considerable effects on the cold, dense bottom water formation of the global thermohaline circulation.

1 Introduction

The rate of sea-ice growth strongly depends on the energy fluxes at the ice or ocean surface. If the total atmospheric heat flux is negative, the ocean is losing heat either directly to the atmosphere or via conduction through an existing sea-ice cover. In the former case frazil ice forms, which aggregates subsequently to a new thin-ice layer under calm conditions. In the latter case basal freezing occurs to balance this heat loss.

In the standard version (v5.0SUBSCRIPTNBelm1) of the regional climate model 'Consortium for Small-scale Model-Climate Limited area Mode' (COSMO-CLM or CCLM;), which is the climate version of the numerical weather prediction model COSMO of the German Meteorological Service, a model grid box is either assumed to be completely covered with sea ice or to be completely ice-free. However, most of the energy exchange between the ocean and the atmosphere occurs over open-water or thin-ice areas, such as leads or polynyas, within an otherwise compact sea-ice cover (Smith et al., 1990; Morales Maqueda et al., 2004). Although the fraction of such areas in polar oceans is relatively small during winter, they are of major importance for the heat budget and of the atmospheric boundary layer (ABL) and the ocean circulation (Heinemann and Rose, 1990; Haid et al., 2015).

The Laptev Sea (Siberia) is a very shallow shelf sea with water depths between 15 and 200 m and comprises an area of about $500 \times 10^3 \text{ km}^2$ (Timokhov, 1994; Krumpen et al., 2013). It is one of the most significant regions where a considerable amount of the total Arctic sea ice is produced (Aagard et al., 1981; Dmitrenko et al., 2009; Dethleff et al., 1998; Willmes et al., 2011; Tamura and Ohshima, 2011; Iwamoto et al., 2014). The newly formed sea ice is subsequently transported by the Transpolar Drift System and accounts for about 20% of the total ice export through Fram Strait (Rigor and Colony, 1997). The Laptev Sea thus plays a key role for future Arctic sea-ice development (Krumpen et al., 2013).

We hypothesise that neglecting subgrid-scale open-water Quasi-stationary latent-heat or flaw polynyas reoccur frequently along the Siberian coast and along the fast ice edge (Dmitrenko et al., 2001; Krumpen et al., 2011; Bareiss and Gørgen, 2005) due to offshore wind stress (Smith et al., 1990; Dmitrenko et al., 2001; Morales Maqueda et al., 2004; Krumpen et al., 2011; Willmes et al., 2011; Dmitrenko et al., 2012). These polynyas are narrow, long bands of open water and/or thin-ice areas could result in an underestimation of the energy transfer and hence in an underestimation of newly grown sea ice, which separate landfast ice from seaward drifting ice on the Siberian continental shelves during winter (Dethleff et al., 1998), predominantly

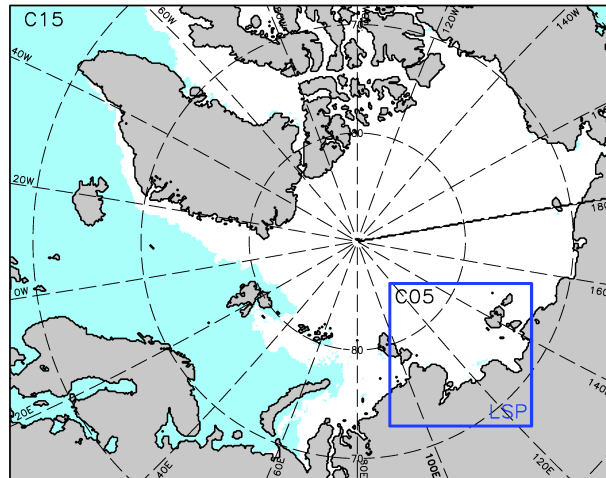


Figure 1. Model domains of COSMO-CLM at a horizontal resolution of 15 km (C015, whole Arctic). The study domain of the Laptev Sea polynyas (LSP) with a resolution of 5 km (C05, blue box) is shown in detail in Fig. 2. The sea-ice extent (white shaded) is from 4 January 2008.

from October until June (Bareiss and G6rgen, 2005). In general, the ice cover in the Laptev Sea can be divided into three regimes: fast ice, pack ice, and flaw polynyas in between (Eicken et al., 2005). This underestimation affects the-

Particularly in winter, sea water at the freezing point is directly exposed to a cold atmosphere, resulting in intense ice formation (Dethleff et al., 1998). Owing to this strong surface heat loss within coastal polynyas frazil ice forms, which is subsequently transported toward the downwind edge of the polynyas (Smith et al., 1990; Morales Maqueda et al., 2004; Krumpfen et al., 2011; Willmes et al., 2010). This process creates a spatial gradient of thin-ice thickness (TIT) increasing from open-water conditions at the windward polyna edge to thicker ice at the downwind side. Here, at the polynya edge, the advected frazil ice accumulates to a thin layer (Martin and Kauffmann, 1981; Krumpfen et al., 2011), which thickens and consolidates before it drifts further offshore. During the ice formation, salt is excluded from the ice matrix and is drained as brine from the sea ice (Krumpfen et al., 2011). This salt input induces haline convection and erodes the density stratification of the underlying water column (Ivanov and Golovin, 2007; Bauch et al., 2009) and if penetrative, dense bottom water forms (Backhaus et al., 1997; Bauch et al., 1995). The long-term mean probability for convective mixing down to the seafloor is only about 20 % in the western and about 70 % in the eastern Laptev Sea (Dmitrenko et al., 2005; Krumpfen et al., 2011), which is owed to the general preservation of the stratification throughout the winter caused by freshwater input from the Lena River during summer (Bauch et al., 2009; Dmitrenko et al., 2005). This density-driven vertical mixing plays a key role in shelf dynamics, producing cold, dense bottom water which contributes to the global thermohaline circulation. Thus the quantification of the sea-ice budget and associated processes connected to the ocean, such as salt release and deep-water formation. production in this area is of global importance.

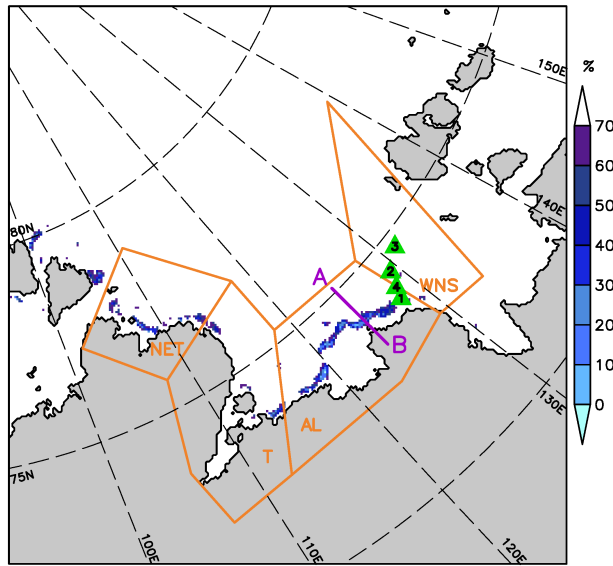


Figure 2. Model domain at 5 km resolution (C05) over the Laptev Sea (approximately 1500 km × 1500 km) with the sea-ice concentration from AMSR-E showing open polynyas ($\leq 70\%$) on 4 January 2008. Four polynya regions are superimposed as orange polygons: north-eastern Taimyr polynya (NET), the Taimyr polynya (T), the Anabar-Lena polynya (AL) and the western New Siberian polynya (WNS). A→B denotes the 214 km long cross-section (magenta) used in section 5. The locations of the four AWS stations are marked with green triangles.

The horizontal resolution of regional climate models is generally too coarse to represent leads and small polynyas explicitly. Therefore, they have to be treated as inhomogeneities of momentum and energy fluxes on a subgrid scale. Heinemann and Kerschgens (2005) investigated three approaches to account for such subgrid-scale inhomogeneities within a model grid box: the (i) aggregation, (ii) mosaic and (iii) tile-approach (TA). In the aggregation approach the parameters for the fluxes (such as roughness length or albedo) are weight-averaged over different surface types within a grid box and then the fluxes are calculated from these grid-scale means. In contrary, in the mosaic approach the fluxes are explicitly calculated on a sub-scale grid and averaged afterwards. In the standard version (v5.0 SUBSCRIPTNBclm1) of the regional climate model 'Consortium for Small-scale Model - Climate Limited area Mode' (COSMO-CLM or CCLM; Rockel et al. (2008)), which is the climate version of the numerical weather prediction model COSMO of the German Meteorological Service (Stappeler et al., 2003), a model grid box is either assumed to be completely covered with sea ice or to be completely ice-free. However, if neglecting subgrid-scale energy fluxes or heat loss from open-water or thin-ice areas, the energy transfer is underestimated and subsequently also the sea-ice production. This underestimation affects the sea-ice budget and associated processes connected to the ocean, such as salt release and deep water formation.

Although the ocean processes are not represented in CCLM, the quantification of sea-ice production can be seen as a proxy for water formation.

To improve the energy exchange over fractional sea ice in CCLM, we modified the standard version with regard to the following points: (i) we implemented the thermodynamic 2-layer sea-ice module of Schröder et al. (2011), (ii) we used daily sea-ice thickness (SIT) fields from the Pan-Arctic Ice-Ocean Modeling and Assimilation System (PIOMAS) data set (Zhang and Rothrock, 2003) as initial data, (iii) we implemented a new albedo-scheme for sea ice based on Køltzow (2007), and (iv) we implemented a tile-approach for the energy balance over fractional sea ice. The TA is a simplification of the mosaic approach, considering only the percentage of different surface types but not their exact location. According to Heinemann and Kerschgens (2005) the TA provides similarly good results as the mosaic approach, but with distinctly less computation time. Thus, we decided to implement this variant. First steps in the direction of a tile-approach in CCLM were made by Van Pham et al. (2014). However, their adjustments were limited to area-weighted albedo values and to surface roughness values within a grid box that is covered with fractional sea ice. In other regional climate models, such as the Polar Weather Research & Forecasting (WRF-Polar-WRF) Model, fractional sea ice is already a default option with the assumption of subgrid-scale open water and with fixed sea-ice concentrations (SIC) and ocean temperatures during a 48 h simulation (Bromwich et al., 2009). However, assumptions have to be made for the subgrid-scale thin-ice thickness, since particularly in winter leads and polynyas are rarely ice-free –

~~To improve the energy exchange over fractional sea ice in CCLM, we modified the standard version with regard to the following points: (i) we implemented the thermodynamic 2-layer sea-ice module of –, (ii) we used daily sea-ice thickness (SIT) fields from the Pan-Arctic Ice-Ocean Modeling and Assimilation System (PIOMAS) data set as initial data, (iii) we implemented a new albedo-scheme for sea ice based on –, and (iv) we implemented a tile-approach for the energy balance over fractional sea ice (Willmes et al., 2011, 2010; Adams et al., 2013).~~

In the following we ~~investigate the sensitivity of ice production (IP) rates~~ quantify the sea-ice production in the Laptev Sea polynyas (~~Siberia~~) Siberia and investigate its sensitivity on the assumptions of thin-ice thickness associated with the tile-approach. Although points (ii)-(iii) represent new modifications to CCLM as well, we accept them as the default option for our reference simulation. The sea-ice module of Schröder et al. (2011) was already successfully applied in the Laptev Sea by Ebner et al. (2011), who could show that polynyas significantly affect the atmospheric boundary layer. More recently, Bauer et al. (2013) calculated sea-ice production rates for this region based on COSMO simulations with an assumed thin-ice thickness of 10 cm (B10) or open water (B00) within polynyas. Their model results showed that the presence of grid-scale thin-ice affects the IP considerably.

The implementation of a TA for subgrid-scale energy fluxes constitutes, from a physical point of view, an improvement of representing polynyas in regional climate models. However, it is unclear how sensitive the energy fluxes ~~and~~, the resulting IP, and the ABL are to the choice of grid-scale and subgrid-scale ice thickness. By varying the ~~ice-thin-ice~~ thickness in a sensitivity experiment, we aim to quantify these uncertainties. As a benchmark for our study we use the IP estimations of Willmes et al. (2011). We further comprise model results of Bauer et al. (2013) and derived IP from Moderate Resolution Imaging Spectroradiometer (MODIS) data.

Table 1. Overview of the performed simulations with COSMO-CLM for the winter period 2007/11–2008/04. The grid-scale thin-ice thickness (TIT) within polynyas (ice concentration: $0 < \text{SIC} \leq 70\%$) is shown in cm and the assumed subgrid-scale TIT is shown in parenthesis. The latter is only required if the tile-approach (TA) is used.

Model run	Δx	Region	TIT [cm]	Description
C15nt-C15	15 km	Arctic	10 (-)	no TA
C05nt-C05-ref	5 km	Laptev Sea	10 (-)	no TA
C05wt0-C05-10/0	5 km	Laptev Sea	10 (0)	with TA
C05wt1-C05-10/1	5 km	Laptev Sea	10 (1)	with TA
C05wt10-C05-10/10	5 km	Laptev Sea	10 (10)	with TA
C05wt50-C05-50/5	5 km	Laptev Sea	50 (5)	with TA
C05wt50-C05-50/1	5 km	Laptev Sea	50 (1)	with TA

This paper is structured as follows: in section 2, a short overview of the model configuration and the study region is given; in section 3 the basics of the sea-ice module are described (see details in appendix A and appendix B). ~~Section 4 shows the calculation of sea ice production.~~ The model is validated with in situ data in section ~~5-4~~ and the effects on the atmospheric boundary layer and on ice production rates are presented in section ~~6 and 7-5 and 6~~ and discussed with respect to remote sensing estimates in section ~~8-7~~. Finally, we ~~draw conclusions in section 9- conclude in section 8.~~

2 CCLM configuration and model domains

2.1 Study area

The Laptev Sea polynyas (LSP), located at the Siberian coast (Fig.1 and Fig.2), are latent-heat polynyas or flaw polynyas. These polynyas are narrow, long bands of open water and/or thin-ice, which separates landfast ice from seaward drifting ice on the Siberian continental shelves during winter. Under such conditions, sea water at the freezing point is directly exposed to a cold winter atmosphere resulting in intense ice formation. The Laptev Sea is a region in which a considerable amount of the total Arctic sea ice is produced. The sea ice is subsequently transported by the Transpolar Drift System and mainly exported through Fram Strait.

The Laptev Sea is usually covered with pack ice from October to June and polynyas recur at quasi-stational locations. Thus we subdivided this region into four polynya regions which have been already used in previous studies, e.g. by the north-eastern Taimyr polynya (NET), the Taimyr polynya (T), the Anabar-Lena polynya (AL) and the western New-Siberian polynya (WNS) (Fig.2). The total area of the masks is $26.19 \times 10^4 \text{ km}^2$.

2.1 Configuration of CCLM

The domain of CCLM (Fig. 1) covers the whole Arctic at a horizontal resolution of 15 km (C15). CCLM was run on 450×350 grid boxes and with 42 vertical layers, whereof 16 are below 2 km height. Nested within, we performed simulations for the Laptev Sea (Fig. 2 and Tab.1) at 5 km resolution (C05) with 260×260 grid boxes and 60 vertical levels, whereof 24 levels are below 2 km height. We subdivided this domain into four polynya regions, which have been already used in previous studies, e.g. by Willmes et al. (2011): the north-eastern Taimyr polynya (NET), the Taimyr polynya (T), the Anabar-Lena polynya (AL) and the western New Siberian polynya (WNS). The total area of the masks is $26.19 \times 10^4 \text{ km}^2$.

The C15 model is forced by ERA-Interim data (Dee et al., 2011) with updates to the lateral boundaries every 6 h. The C05 ~~model is~~ models are then forced by the output of C15 with an update frequency of 1 h. The models were run in a forecasting procedure for the winter period November 2007 to April 2008 (182 days in total). They were restarted every simulation day at 18 UTC and simulated the following 30 hours. Thereby the initial sea-ice conditions (see section 3.2) were prescribed to the sea-ice concentration and thickness of the following day. The first 6 hours were cut off as spin-up. The simulation output (00-23 UTC) was stored at a temporal resolution of 1 hour.

Surface fluxes ~~are were~~ calculated by a bulk transfer scheme with a stability ~~dependency~~ dependence (Louis, 1979) (see appendix B3). The vertical diffusion ~~is was~~ parameterized by a level-2.5 closure scheme (Mellor and Yamada, 1974) based on a prognostic equation for turbulent kinetic energy (TKE). Radiation processes ~~are calculated hourly using were calculated hourly using~~ the Ritter and Geleyn (1992) scheme extended for ice-clouds. We applied a Runge-Kutta scheme of 3rd order (Wicker and Skamarock, 2002). Additionally, a fast-wave solver for sound and gravity waves was used (Baldauf, 2013). All simulations were run without spectral nudging. ~~We assumed a grid-scale ice thickness of 10 cm within polynyas, except for two sensitivity runs where 50 cm have been assumed (Tab.1, and see section 3.2).~~

The ~~15 km C15~~ simulation was performed without a TA (~~C15nt~~) in order to introduce effects from the TA only through the 5 km simulations. In case of C05, we performed a reference simulation in the Laptev Sea area without a TA (~~C05nt~~C05-ref) and five sensitivity simulations with the TA. While the sea-ice thickness outside the polynyas was specified as explained in section 3.2, the ice thickness within the polynya areas has to be prescribed. For C15 and C05-ref the ice thickness in polynya areas is generally 10 cm, but we assume 1 cm thin ice at polynya grid boxes in C05-ref, where the sea-ice concentration is 0%. This assumption is motivated by the fact that open-water areas particularly produce new ice and are hence rarely free of ice in winter. Further, such areas occur mostly at the windward side of polynyas, which is only a small fraction of the entire polynya area.

For ~~C05nt~~ and three of the five sensitivity simulations we assumed also a grid-scale ice thickness of 10 cm for polynyas and either assumed subgrid-scale open water (~~C05wt0~~C05-10/0) or a subgrid-scale TIT of 1 cm (~~C05wt1~~or C05-10/1) and 10 cm (~~C05wt10~~C05-10/10), respectively. The fourth and fifth sensitivity simulations were configured with a grid-scale ice thickness of 50 cm and a subgrid-scale TIT of 5 cm (C05-50/5) or 1 cm (C05-50/1). See Tab. 1 for an overview of the simulations. The assumption of 10 cm TIT originates from the fact that the mean TIT below 20 cm, derived from MODIS data, is ≈ 10 cm (Willmes et al., 2011). In ~~previous studies~~ a previous study by Bauer et al. (2013) this value was assumed to be the most

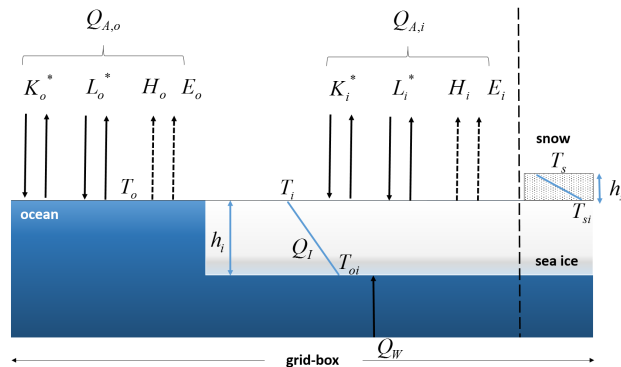


Figure 3. Scheme of the modified two-layer thermodynamic sea-ice module of Schröder et al. (2011), extended with a tile-approach for fractional sea ice. Sea ice is distinguished as bare ice or as snow covered ice (with $h_s = 0.1$ m snow depth if sea-ice thickness $h_i > 0.2$ m). The subgrid-scale open ocean fraction is either ice-free (C05-10/0) or assumed to be covered with 1 cm (C05-10/1, C05-50/1), 5 cm (C05-50/5) or 10 cm thin-ice (C05-10/10). In the reference simulation (C05-ref), grid boxes with 0% sea-ice concentration are covered with 1 cm grid-scale thin-ice. If the index k denotes either sea-ice (i) or ocean (o), then $Q_{A,k}$ is the total atmospheric heat flux, K_k^* is the net shortwave and L_k^* the net longwave radiation. H_k and E_k are the sensible and latent heat fluxes. T_k is the surface temperature, h_i the ice thickness, T_{oi} the ice-ocean interface temperature and T_{si} the snow-ice interface temperature. Q_I denotes the conductive heat flux through the ice and Q_W the turbulent heat flux from the oceanic mixed layer into the ice.

realistic one for the ice thickness within the polynyas. The first three sensitivity simulations investigate the effect of the TA, if even thinner ice is assumed. The C05-50/5 and C05-50/1 runs are motivated by the fact that fractional the sea-ice cover in the marginal ice zone consists of thicker ice floes (detected by microwave satellite sensors), and thin-ice of (the assumed 5 cm or 1 cm, respectively), which is not detected by microwave sensors.

For C05nt we further assume 1cm thin ice at polynya grid boxes where the Although this is a crude simplification to the real sea-ice concentration is exactly 0%. This assumption is motivated by the fact that open water areas particularly produce new ice and are hence rarely free of ice thickness, it is suited for our purpose to investigate the impact on the magnitude of ice production and on the modification of the ABL. We intended to consider sea ice in a computational cheap approach that still incorporates realistic thermo-dynamical processes. For a more sophisticated approach, a full dynamic-thermodynamic sea-ice model needs to be coupled to CCLM.

3 The two-layer thermodynamic sea-ice module

3.1 Basic module

10 In this section the sea-ice module (Fig. 3) is briefly described. The module considers a snow and sea ice layer and was described and originally implemented in the COSMO model by Schröder et al. (2011). It is based on the module of Mironov et al. (2012).

For this study it is reimplemented within the version 5.0_clm1 of CCLM extended with the K \ddot{o} ltzow sea-ice albedo scheme (see appendix A). More important for this study is the implementation of a tile-approach for the surface energy balance over fractional sea ice (see appendix B). The module and hence sea-ice growth calculation is only applied to grid boxes with an initial sea-ice cover. Formation of grease ice in open water is not parameterized in CCLM, which is even a difficult task for stand-alone sea-ice ocean models. Nevertheless, a more sophisticated parameterization has been recently developed by Smedsrud and Martin (2015). For this reason we ~~calculate~~calculated sea-ice production in a post-processing step (see section 3.1).

5 The module assumes a constant ocean/ice interface temperature of $T_{oi} = -1.7^{\circ}\text{C}$, i.e. T_{oi} is not dependent on salinity. A temperature of -1.7°C assumes approximately a salinity of ~~31.1PSU~~31.1psu. The module ignores turbulent heat fluxes from the ocean at the lower boundary. Heat conductivity parameters are $2.3\text{W m}^{-1}\text{K}^{-1}$ for sea ice and $0.76\text{W m}^{-1}\text{K}^{-1}$ for snow. The module assumes a snow cover of $h_s = 0.1\text{m}$ if the ice thickness exceeds a threshold $h_i > h_c$ with $h_c = 0.2\text{m}$.

3.2 Sea-ice concentration and thickness for initial conditions

The sea-ice concentration (SIC) is prescribed from Advanced Microwave Scanning Radiometer-Earth Observing System (AMSR-E) data (Spreen et al., 2008), provided by the University of Bremen. The original data sets are available on a daily basis at a horizontal resolution of 6.25 km. In order to use them for CCLM, we interpolated the SIC fields onto the C15 and C05 grid, respectively, by a bilinear approach for every simulation day. All grid boxes with $\text{SIC} \leq 70\%$ are treated as polynyas (Massom et al., 1998; Adams et al., 2011; Preu \ddot{u} er et al., 2015a). Realistic polynya areas are retrieved by using this threshold, as shown by Adams et al. (2011) in comparison to a polynya signature simulation method (Markus and Burns, 1995).

15 Sea-ice thickness (SIT) is taken from the Pan-Arctic Ice-Ocean Modeling and Assimilation System (PIOMAS) data set (Zhang and Rothrock, 2003). The PIOMAS data are available at a daily basis with a mean grid spacing of about 25 km (Hines et al., 2015). These daily fields were masked with the daily SIC fields to obtain consistent sea-ice extents. Thereby sea ice outside the AMSR-E mask was removed and grid boxes which were ice-free in the daily PIOMAS fields but covered with ice in the mask were assigned with an interpolated SIT from a nearest neighbour method.

Schweiger et al. (2011) state that PIOMAS seems to overestimate thin-ice thickness and underestimates thicker ice. Nevertheless, the overestimation should not be problematic in our application, since we have to set TIT for daily fields according to AMSR-E data. Underestimations of thicker ice is of a minor concern to our study due to the focus on areas with thin ice. Using this setup, the sea-ice thickness fields are much more realistic than in previous studies, where a constant thickness of 1 m was assumed outside polynyas (Ebner et al., 2011; Schr \ddot{o} der et al., 2011; Bauer et al., 2013).

4 Estimation of sea-ice production

3.1 Estimation of sea-ice production

In accordance to previous model or satellite-based studies, the sea-ice production (IP) was calculated in a post-processing step using the energy balance (Bauer et al., 2013; Ebner et al., 2011; Willmes et al., 2011). This approach assumes that if the

Table 2. Overview of the four automatic weather stations (AWS) with hourly measurements which were deployed during the Transdrift XIII-2 expedition from 11–29 April 2008 (Heinemann et al., 2009). See the location of the AWS stations in Fig. 2.

Station	Location	Measured period (UTC)
AWS1	128.16 °E 73.80 °N	11 Apr. 2008 07:00 – 26 Apr. 2008 12:00
AWS2	129.32 °E 74.39 °N	12 Apr. 2008 04:00 – 29 Apr. 2008 03:00
AWS3	131.25 °E 74.67 °N	14 Apr. 2008 06:00 – 29 Apr. 2008 01:00
AWS4	128.61 °E 74.05 °N	24 Apr. 2008 06:00 – 28 Apr. 2008 02:00

Table 3. Statistical comparison of 2m temperature, 10m wind speed (3m in case of the AWS) and net radiation ($K^* + L^*$) of the four AWS and the C05 simulations: C05-ref (reference), C05-10/0 (open-water), and C05-50/1 (realistic). Hourly means are denoted by \bar{x} and standard deviations are denoted by σ . The Pearson correlation coefficient (r) was calculated with the AWS and C05 time series. The critical correlation coefficient ($\alpha = 5\%$), which is depending on the sample size of the AWS time series, is between 0.1 and 0.2. In addition, the resulting p-values (p) of two-sided t-tests ($\alpha = 5\%$) are shown. Significant differences are marked with *. Data pairs with missing values in the AWS data or where the sea-ice concentration is $< 95\%$ were removed prior to the analyses.

Data

AWS1

$\overline{C05_{nt}} - \overline{C05_{ref}}$

$C05_{wt10} - 20.60 \ 1.91 \ 0.79 \ 0.48 \ 3.42 \ 1.56 \ 0.75 \ 0.74 \ -30.18 \ 26.11 \ 0.80 < 0.01^* \ C05_{wt1} - 20.54 \ 1.92 \ 0.79 \ 0.66 \ 3.46 \ 1.58 \ 0.75 \ 0.55 \ -30.05 \ 26.25 \ 0.80 < 0.01^* \ C05_{wt0} - \overline{C05_{10/0}}$
 $C05_{50/5} - 20.58 \ 1.91 \ 0.79 \ 0.55 \ 3.43 \ 1.57 \ 0.75 \ 0.68 \ -30.12 \ 26.14 \ 0.80 < 0.01^* \ C05_{50/1}$

AWS2

$\overline{C05_{nt}} - \overline{C05_{ref}}$

$C05_{wt10} - 20.54 \ 2.15 \ 0.78 < 0.01^* \ 3.34 \ 1.33 \ 0.69 < 0.01^* \ -28.36 \ 24.97 \ 0.75 < 0.01^* \ C05_{wt1} - 20.50 \ 2.12 \ 0.79 < 0.01^* \ 3.35 \ 1.35 \ 0.69 < 0.01^* \ -28.72 \ 25.15 \ 0.75 < 0.01^* \ C05_{wt0} - \overline{C05_{10/0}}$
 $C05_{50/5} - 20.52 \ 2.14 \ 0.79 < 0.01^* \ 3.35 \ 1.34 \ 0.69 < 0.01^* \ -28.43 \ 24.92 \ 0.76 < 0.01^* \ C05_{50/1}$

AWS3

$\overline{C05_{nt}} - \overline{C05_{ref}}$

$C05_{wt10} - 19.53 \ 3.06 \ 0.86 \ 0.09 \ 3.16 \ 1.46 \ 0.70 < 0.01^* \ -23.54 \ 28.65 \ 0.70 < 0.01^* \ C05_{wt1} - 19.47 \ 3.08 \ 0.86 \ 0.13 \ 3.17 \ 1.46 \ 0.69 < 0.01^* \ -23.52 \ 28.76 \ 0.70 < 0.01^* \ C05_{wt0} - \overline{C05_{10/0}}$
 $C05_{50/5} - 19.50 \ 3.08 \ 0.86 \ 0.11 \ 3.16 \ 1.46 \ 0.70 < 0.01^* \ -23.39 \ 28.74 \ 0.70 < 0.01^* \ C05_{50/1}$

AWS4

$\overline{C05_{nt}} - \overline{C05_{ref}}$

$C05_{wt10} - 16.31 \ 3.28 \ 0.65 < 0.01^* \ 4.64 \ 2.28 \ 0.92 \ 0.14 \ -34.31 \ 28.26 \ 0.73 < 0.01^* \ C05_{wt1} - 16.25 \ 3.26 \ 0.66 < 0.01^* \ 4.72 \ 2.38 \ 0.91 \ 0.09 \ -34.21 \ 28.46 \ 0.74 < 0.01^* \ C05_{wt0} - \overline{C05_{10/0}}$
 $C05_{50/5} - 16.26 \ 3.29 \ 0.65 < 0.01^* \ 4.65 \ 2.29 \ 0.92 \ 0.13 \ -34.24 \ 28.43 \ 0.73 < 0.01^* \ C05_{50/1}$

water within a polynya is at the freezing point, all energy loss to the atmosphere through the ocean surface is compensated by

freezing. Hence sea-ice growth only occurs if the total atmospheric energy flux over ice (index $k = i$) or ocean (index $k = o$) $Q_{A,k} = K_k^* + L_k^* + H_k + E_k$ is negative, i.e. the ocean loses heat:

$$\frac{\partial h_i}{\partial t} = -\frac{Q_{A,k}}{\rho_i \cdot L_f}, \quad (1)$$

15 with h_i the sea-ice thickness, $\rho_i = 910 \text{ kg m}^{-3}$ the density of sea ice and $L_f = 0.334 \times 10^6 \text{ J kg}^{-1}$ the latent heat of fusion. We restricted this estimation to the four polynya areas in the Laptev Sea (see Fig. 2), which are identical to those of Willmes et al. (2011). Hence, direct comparisons of our results with estimations from remote sensing ~~are~~ were possible.

We further calculated the IP using the MOD/MYD29 sea-ice surface temperature product (Hall et al., 2004; Riggs et al., 2006) derived from MODIS Terra and Aqua data. In combination with ERA-Interim data (~~2 m~~-temperature, 2 m temperature,
5 2 m dew point temperature, 10 m horizontal wind components and pressure at mean sea level), an energy balance model (e.g. Yu and Lindsay, 2003; Adams et al., 2013; Preußer et al., 2015b, a) was applied to derive thin-ice thicknesses up to 0.2 m at a horizontal resolution of about 2 km. We refer to this estimation as MODIS2km. The turbulent fluxes of sensible and latent heat were calculated by an iterative bulk approach (Launiainen and Vihma, 1990) based on the Monin-Obukhov similarity theory. Thereby, the turbulent exchange coefficient C_H is ~~variable in time~~ a function of stability, and of the roughness length
10 for momentum and for heat, respectively (Doms et al., 2011). Shortwave radiation is not considered as the method is restricted to ~~wintertime nighttime conditions during winter~~. This method is only applicable to clear sky conditions, as clouds and fog impede an estimation of sea-ice surface temperature (Riggs et al., 2006). Therefore the number of useful swaths per day is variable. For instance, in the Laptev Sea there are about 10 to 14 swaths per day (2002/03 to 2014/15 (Nov.-Mar.)).

Cloud-induced gaps in our daily sea-ice surface temperature and thin-ice thickness composites were filled by a spatial
15 feature reconstruction procedure (Paul et al., 2015; Preußer et al., 2015a). This method interpolates information of previous and subsequent days to fill gaps caused by cloud-cover. Based on these corrected composites and using the method described in Preußer et al. (2015b), ice production rates were calculated for each pixel with an ice thickness $\leq 0.2 \text{ m}$, i.e. for polynya areas.

In a sensitivity analysis of this method (without the spatial feature reconstruction), Adams et al. (2013) stated an uncertainty for the ice-thickness retrieval of $\pm 1.0 \text{ cm}$, $\pm 2.1 \text{ cm}$ and $\pm 5.3 \text{ cm}$ for thin-ice classes of 0 – 5 cm, 5 – 10 cm and 10 – 20 cm, respectively. Therefore, we constrained our analysis to ice thicknesses $\leq 0.2 \text{ m}$, as this range is regarded as sufficient to get reliable results for ice production (Yu and Rothrock, 1996; Adams et al., 2013).

Furthermore, we compared our results to the estimations of Willmes et al. (2011). In their study they used a constant
5 transfer coefficient for heat $C_H = 3 \times 10^{-3}$ to calculate H and E from AMSR-E data and using MODIS thin-ice distributions and National Centers for Environmental Prediction/National Center for Atmospheric Research (NCEP/NCAR) reanalysis data ($2.5^\circ \times 2.5^\circ$) as atmospheric forcing for an energy balance model. However, we omitted the most western polynya mask of their study and ~~compare~~ compared the IP only to the four remaining masks shown in Fig. 1 and Fig. 2.

We also compared our IP estimations to model-based estimations of Bauer et al. (2013). Bauer et al. (2013) conducted two
10 COSMO simulations at 5 km horizontal resolution (without a tile-approach) for the same winter 2007/08 in the Laptev Sea.

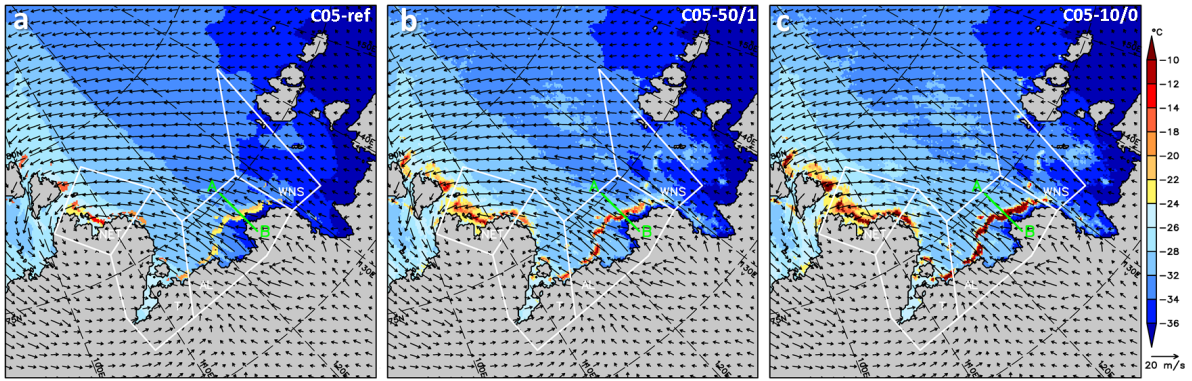


Figure 4. Surface temperature and 10 m wind field on 4 January 2008 at 15 UTC in (a) C05-ref (reference), (b) C05-50/1 (realistic), and (c) C05-10/0 (open-water). The green line marks the cross-section A→B used for Fig. 5.

One simulation assumed a grid-scale thin-ice thickness of 10 cm within polynyas (B10) and one simulation assumed open-water (B00). Both simulations further assumed a sea-ice thickness of 1 m outside polynyas. Both simulations were forced by a 15 km COSMO simulation, which was nested within the output of the global GME model.

4 Verification with in situ data

- 15 The ~~results of the five model output of the reference and the five sensitivity~~ simulations were first ~~compared to verified with~~ in situ data ~~in order to verify the model configurations~~. During the Transdrift XIII-2 expedition from 11 April to 29 April 2008 four automatic weather stations (AWS, Tab. 2) were deployed on the fast ice of the western New Siberian Polynya (WNS, see Fig 2) (Heinemann et al., 2009). The AWS measured wind speed and direction at 3 m height with an accuracy of 2% in speed and 3° in direction; air temperature and relative humidity at 2 m height with an accuracy of 0.5 K and 4%, and pressure with an accuracy of 1 hPa. Furthermore, net radiation was measured by a net radiometer with an accuracy of 5 W m⁻².
- 20

Here, we compared hourly ~~CCLM-C05~~ data with the AWS data. In order to judge whether the simulations deviate significantly from the AWS data two-sided t-tests were performed ($\alpha = 95\%$). ~~The statistical comparison was~~ ~~The statistical comparisons were~~ only performed for data pairs ~~with no without~~ missing values and only for days when the SIC was > 95%. This limitation is necessary because the time series of CCLM represent spatial averages of a grid box, whereas the AWS time series are point data on a solid ice cover. If the SIC of CCLM is < 100% then the grid average automatically differs from the station time series, which always represent conditions at 100% SIC.

25

~~The time series comparison of AWS1 and the CCLM simulations are shown in Fig. 5. Since the course of the time series of AWS2-4 and CCLM are qualitatively similar to AWS1, we only show~~ Tab. 3 shows the results for the reference simulation (C05-ref) and two sensitivity simulations: C05-10/0 (subgrid-scale open-water) and C05-50/1 (realistic assumptions). In the

30 remainder of the manuscript, we concentrate on the comparison of AWS1. A complete summary of all comparisons is compiled in Tab. 3 these three simulations. Since the comparison was made only over a solid sea-ice cover, the other simulations showed very similar results (not shown).

In Fig. general, the inter-model differences are minor for all variables. The comparison for the 2.5 m temperature shows that the C05 simulations are generally able to reproduce the observed temperatures during the measurement period. The temporal correlation is about $r = 0.8$, except for the comparison with AWS4. The bias is about -1°C for AWS2-3, less for AWS1 is shown. Although the 2 m temperature of the CCLM simulations principally follows the curve progression of the AWS stations ($r \approx 0.8$, Fig. 5a), distinct differences are visible. On the first 7 days, CCLM is too warm during late evening and at night-time, while thereafter the temperature peaks at midday are underestimated. Overall, the mean temperature differs only up to 0.2°C (not significant), but the standard deviation is only about 60% of the observation (see Tab. 3). The inter-model comparisons show no distinct differences, which is also confirmed by the Taylor plot (Fig. and about -3°C for AWS4. Except for the latter, C05 underestimates the variability of the 2.5 m temperature. This might be caused by the assumptions made on snow properties in C05. Although the t-tests are significant for differences of about 1°C , this difference is sufficient for our analysis keeping in mind that grid box averages were compared with point data.

In case of wind speed there is a good agreement ($r = 0.75$, Fig. 5e-d $r > 0.7$), although we compare compared 10 m wind speed of CCLM with measurements at 3 m height. The mean and standard variance are both in accordance with the AWS1 station (Tab. 3 and Fig. 5d). Reversely AWS data, although significant for differences $\geq 0.4 \text{ m s}^{-1}$. Inversely, this agreement implies that CCLM underestimates wind speeds at 10 m, although we do not have reference data at 10 m for a verification.

15 Significant differences were found for the comparison of the net radiation (Tab. 3, Fig. 5e-f). Although the temporal correlation is high ($r \approx 0.8$ $r > 0.7$), the mean of CCLM is about $12-13 \text{ W m}^{-2}$ lower than the observed -17.87 W m^{-2} . These differences in the mean, and a slight underestimation of 5 W m^{-2} of the standard deviation result in significant test results. A visible inspection of Fig. 5e shows a good agreement on some days C05 is about $13-22 \text{ W m}^{-2}$ lower than observed meaning a slightly too high heat flux through the sea ice cover. This difference might be caused by the assumption on the sea-ice properties (e.g. 14-16 Apr.), but a systematic shift to more negative values on other days (e.g. 12-13 Apr.). This might be caused by errors in the cloud cover, which we unfortunately cannot compare because there are no measurements at the stations locations. The comparison with AWS2-3 shows temperature differences of about -0.5°C to -1°C , higher wind speeds of about $+0.4 \text{ m s}^{-1}$ to $+0.7 \text{ m s}^{-1}$ and differences of -13 W m^{-2} to -14 W m^{-2} for net radiation a constant temperature at the ice-ocean interface) or by the slight cold bias of the ABL above the sea ice.

25 Albeit some deviations CCLM is able to reproduce the basic conditions of the near-surface variables during this period with our chosen configurations. However, the reasons for these deviations need further investigation and with longer time series.

5 Effects of the tile-approach on the atmospheric boundary layer

5.1 Case study on 4 January 2008

The effects of the TA are exemplified for a case study on 4 January 2008. On this day a low was located over the Taimyr peninsula in the western Laptev Sea. The large pressure gradient generated strong, prevailing off-shore winds, which caused a large opening of polynyas at the fast-ice edge in the Laptev Sea (Fig. 6a4). The 10 m wind speed reached 10 to 15 m s⁻¹ and was blowing offshore over the Anabar-Lena polynya (AL). The associated sea-ice concentrations for that day are shown in Fig. 2. Within polynyas, the SIC is about ~~10%–0%~~ to 70%.

5.1.1 Surface temperature

5 The surface temperatures (T_{sfc}) of the ~~CELM-CO5~~ simulations at 15 UTC (Fig. 64) show a clear signal of the polynyas. Within the AL polynya the surface temperatures are -22°C to -24°C in ~~C05nt-CO5-ref~~ (Fig. 64a), which is ~~6–16~~ +6 to +16 $^{\circ}\text{C}$ warmer than the surrounding ~~thicker ice, fast and pack ice.~~

Furthermore, T_{sfc} is about ~~2~~ +2 $^{\circ}\text{C}$ warmer at the ~~lee-downwind~~ side than at the windward side. ~~Stronger horizontal temperature gradients result for the NET polynyas. The first sensitivity run, C05wt10 (Fig. 6d), shows similar temperatures within polynyas and a similar wind field. Slightly warmer temperatures occur at the polynya margins, in particular in areas with > 70% SIC. In these areas, the subgrid-scale open water is covered with 10 cm thin-ice, resulting in warmer grid average temperatures compared to C05nt. If a subgrid-scale~~ This is, however, not realistic compared to nature. One would expect higher temperatures at the windward side due to the spatial gradient of the thin-ice with the thinnest or even open water at the windward side. Since in C05-ref a homogeneous thin-ice thickness of 1 cm is assumed (C05wt1, Fig. 6b), the surface temperatures within the polynyas become warmer than -18°C , an considerable increase of up to $+6^{\circ}\text{C}$ compared to C05nt. A further warming occurs at the margins of the polynyas, in particular visible for the NET polynyas, and over the pack ice, where the SIC is 100%. A similar picture results for C05wt0 (Fig. 106e). The temperature within polynyas even reaches values warmer than -10°C cm is assumed within the polynya, this effect is not represented in the simulation.

Much higher surface temperatures were simulated by all sensitivity simulations. As an upper limit, C05-10/0 simulates $\geq 10^{\circ}\text{C}$ higher surface temperatures. This increase of surface temperature is in accordance with results of Bromwich et al. (2009), who found an increase of 14°C for sea-ice concentrations of about 60% in winter. ~~These two effects lead to an increased area where oceanic heat is exchanged with the atmosphere. While T_{sfc}~~ In the more realistic configuration of C05-50/5 (Fig. 6e) is lower than in C05nt, C05-50/1 (Fig. 6f) shows warmer temperatures are about $\leq 10^{\circ}\text{C}$ warmer. The warmest areas within the polynya tend to be at the windward side now, which is owed to the TA and the thereby considered spatial thin-ice gradient. Another effect, which becomes visible, is that the marginal area of the polynyas with warmer T_{sfc} as well, ~~which are in between of C05wt10 and C05wt1~~ increases with the use of TA. This effect is most obvious for the NET polynyas. This increases the area where heat is transferred from the ocean into the atmosphere and causes smooth transitions from the fast or pack ice to the polynyas. An increased heat loss has to be balanced by an increase in frazil ice production.

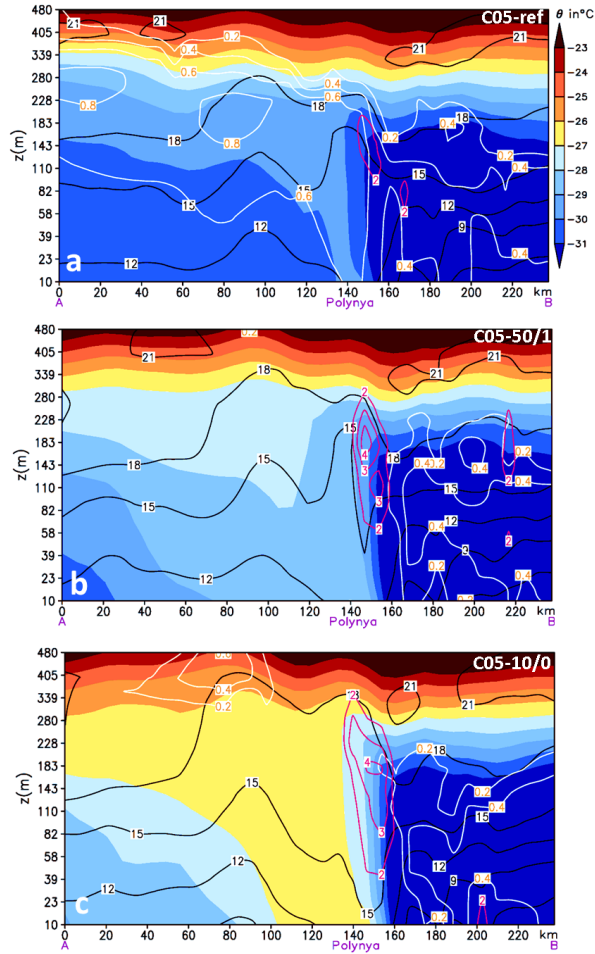


Figure 5. Vertical cross-sections of the potential temperature Θ , horizontal wind speed (black contour lines), turbulent kinetic energy (TKE in $m^2 s^{-2}$, magenta contour lines), and cloud fraction (white contour lines and orange labels) on 4 January 2008 at 15 UTC for (a) C05-ref (reference), (b) C05-50/1 (realistic), and (c) C05-10/0 (open-water). The horizontal distance is about 240 km and the location of the cross-section A (pack ice) \rightarrow B (fast ice) is shown in Fig. 2.

5.1.2 10-m-10 m wind speed

25 The 10-m-wind-speed-in-C05nt (wind speed is the main driver for mixing in the ABL above polynyas and mainly controls the sensitive heat flux until the warming of the ABL reduces the vertical temperature gradient and thus the sensitive heat loss and subsequently the ice production. Fig. 6a) is about $14-18 m s^{-1}$ over the AL polynya. In C05wt0 (Fig.4 shows the 10 m wind speed and direction on 4 January 2008 at 15 6eUTC. In the reference run (C05-ref) the wind speed increases by

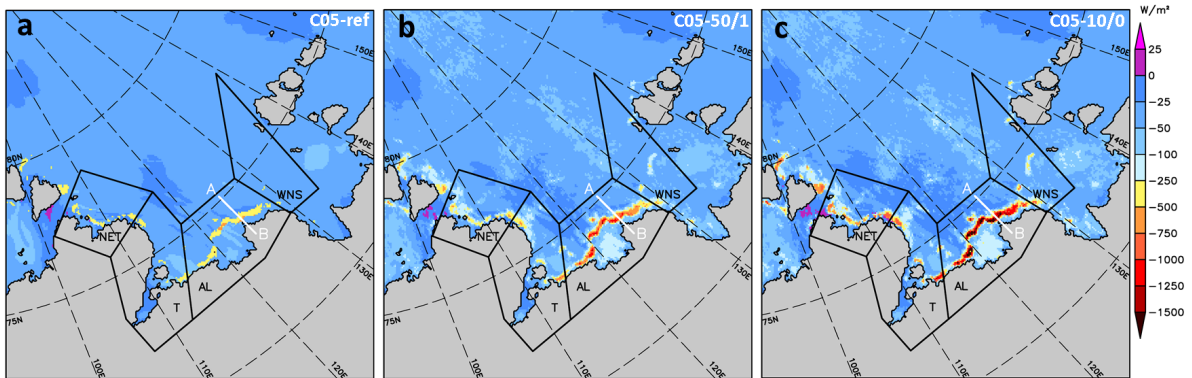


Figure 6. Total atmospheric energy flux on 4 January 208 at 15 UTC in (a) C05-ref (reference), (b) C05-50/1 (realistic), and (c) C05-10/0 (open-water). Negative fluxes are directed upwards. The white line marks the cross-section A→B used for Fig. 5.

2—5 m s⁻¹, less for C05wt1 (Fig. 6b), C05wt10 (Fig. 6d), C05-50/5 and C05-50/1 (Fig. 6e-f). These results are above the AL polynya is about 14 to 18 m s⁻¹. The wind speed slightly increases in the sensitivity simulations (+2 to +5 m s⁻¹), which is in accordance with idealized studies conducted by Ebner et al. (2011) (see Fig 5c therein). Ebner et al. (2011) concluded that the increase in wind speed results in an increased net ice production, despite an increased boundary layer warming. The increase in near-surface wind speed causes a larger momentum flux (not shown, but see section 5.1.3 for the turbulent kinetic energy (TKE)) and higher energy loss from the ocean. Furthermore, although not represented in the present CCLM model, higher wind speeds increase the sea-ice drift within polynyas, so that newly formed ice is likely to drift faster, so that a strong heat loss is maintained. Both processes are expected to increase the IP. However, the latter issue has to be investigated by coupled atmosphere/sea-ice/ocean model simulations. A similar effect, although less pronounced, was simulated by C05wt1 (Fig. 6b), but no distinct deviations of the wind were found for C05wt10, C05-50/5, and C05-50/1.

5.1.3 Total atmospheric energy flux

The exchange of heat from the ocean to the atmosphere is summarized in the total atmospheric energy flux Q_A (Fig. 7). In C05nt (Fig. 7a) Q_A is slightly negative (-25 W m^{-2} to -100 W m^{-2}) over the pack ice, and reaches about -500 W m^{-2} over the polynyas (negative values indicate upward fluxes). Similar values within the polynyas result for C05wt10 (Fig. 8d), with slightly more negative values along the polynya margins, so that there is a transition from thin-ice to the pack ice. Q_A becomes considerably more negative over polynyas in C05wt0 with $< -1000 \text{ W m}^{-2}$ (Fig. 7c), in C05wt1 with $\approx -1000 \text{ W m}^{-2}$ (Fig. 7b), in C05-50/5 with $\approx -750 \text{ W m}^{-2}$ (Fig. 7e), and -750 W m^{-2} to -1000 W m^{-2} in C05-50/1 (Fig. 7f). Thus if the TA is used with our assumed ice thicknesses, more heat is released into the atmospheric boundary layer.

Model Q_A H E L* K* ΔT Δq ($^{\circ}\text{C}$) (10^{-4} kg/kg) C05nt 252.5 166.7 41.0 67.4 22.6 6.7 6.2 % Q_A 66.0%
 5 16.2% 26.7% 8.9% C05wt10 246.3 161.6 39.8 67.8 22.8 6.5 5.8 % Q_A 65.6% 16.1% 27.5% 9.3% Δ

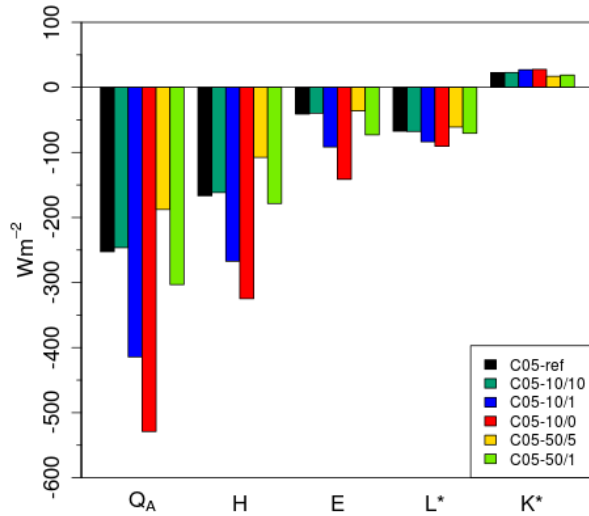


Figure 7. Temporal means of the energy balance Q_A and its components averaged over polynya grid boxes for the winter period 2007/08. For the averaging at least 9 grid boxes in the model domain had to be polynyas to include them in the calculation.

~~-2.5% -3.1% -2.9% +0.6% +0.9% -3.0% -6.5%~~ C05wt1 -414.4 -267.3 -91.6 -82.6 27.1 -9.8 -10.0% Q_A -64.5%
~~22.1% 19.9% -6.5%~~ Δ +64.1% +60.3% +123.4% +22.6% +19.9% +46.3% +61.3% C05wt0 -529.0 -324.8 -141.3
~~-90.6 27.7 -11.6 -10.4%~~ Q_A -61.4% 26.7% 17.1% -5.2% Δ +109.7% +94.8% +244.6% +34.4% +22.6% +73.1% +67.7%
 C05-50/5 -187.7 -107.7 -36.0 -61.1 17.1 -4.1 -0.3% Q_A -57.4% 19.2% 32.6% -9.1% Δ -25.9% -35.4% -12.2%
 10 ~~-9.3% -24.3% -38.8% -95.2%~~ C05-50/1 -303.2 -178.6 -73.0 -70.6 19.0 -6.5 -0.7% Q_A -58.9% 24.1% 23.3%
~~-15.9%~~ Δ +20.1% +7.1% +78.0% +4.7% -6.3% -3.0% -88.7%

5.1.3 Vertical cross-sections

Fig. 8 shows ~~5 shows vertical~~ cross-sections of the potential temperature Θ , the horizontal and vertical wind speed, the cloud area fraction and the turbulent kinetic energy (TKE) over the AL polynya. In ~~C05wt~~ ~~C05-ref~~ (Fig. 85a) Θ is about -29°C at
 15 10m height over the polynya, about -30°C about the pack ice, and colder than -31°C over the fast ice. The boundary layer is stably stratified over the pack and the fast ice but ~~well-mixed and warmer~~ over the polynya. ~~These warm air masses reach heights of 150-200m downstream the polynya.~~ TKE values of up to ~~2-2.5~~ m^2s^{-2} are simulated over the transition from fast ice to the polynya (at km 140-160) and downstream the polynya opening (at km 100-120).

A similar ~~a well-mixed~~ convective boundary layer of the polynya is simulated by C05wt10 (Fig.8d), except that the
 20 air downstream the polynya is about 1°C warmer close to the surface, because of the warmer surface temperatures at the

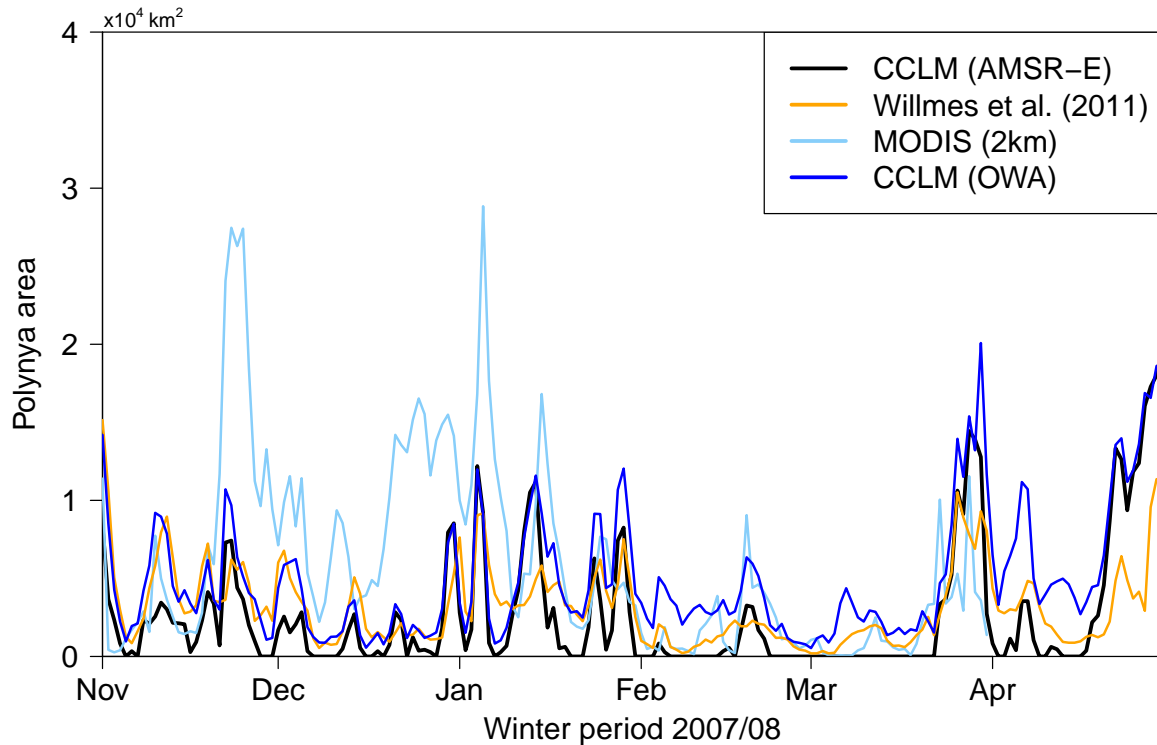


Figure 8. Total daily polynya area interpolated from AMSR-E (using a 70 % threshold) onto the CCLM 5 km grid in the Laptev Sea for the winter period 2007/08 aggregated for the four polynya masks. In addition, the polynya area plus open-water area (OWA = 1 – SIC) for the polynya masks is shown. Based on remote sensing the polynya areas estimated from Willmes et al. (2011) and MODIS2km data are shown. The total area of the polynya masks is $26.19 \times 10^4 \text{ km}^2$.

downstream margin of the polynya and the associated enhanced heat loss. Thus, the TA increases the area and the intensity of heat loss from polynyas, so that the boundary layer warms compared to C05nt ($+2^\circ\text{C}$ in C05wt1 (Fig. 8e) and $+3^\circ\text{C}$ in C05wt0 (Fig. 8b)). The increased heat supply triggers convection above the polynya. This increases the turbulent kinetic energy (TKE) (Fig. CBL) has developed, capped by an inversion at approximately 300 to 500 m up to $> 4 \text{ m}^2 \text{ s}^{-2}$ due to convection, enhances mixing and the upward vertical motion in height. Comparing the cross-sections for the three shown model configurations, it becomes obvious that the assumptions on the thin-ice within a polynya has considerable effects on the ABL.

25

As mentioned earlier, the onset of the CBL at the windward polynya edge is displaced to the polynya interior in the reference simulation (C05-ref) compared to the sensitivity simulations. This is owed to the too thick ice in this area, preventing a large enough heat transfer and hence vertical mixing. This is also reflected in the low values of TKE compared to twice as high

30 values for the sensitivity runs. In the open-water configuration (C05-10/0) the CBL is thus about 3°C warmer than in the reference run. The warm air spreads as a plume downstream the polynya and can be tracked several hundred kilometres over the pack ice (not shown). In C05-50/5 (Fig.8e) the convective boundary layer particularly downstream of the polynya is about 1°C warmer than in C05nt, and in C05-50/1 (Fig.8f) about 2°C . The values of TKE and upward vertical motion are similar to those of C05wt1

One might suspect that the warmer CBL of the sensitivity simulations might lead to a reduced vertical temperature gradient over the polynya and thus to a negative feedback for the surface sensible heat flux and thus ice production. This is not the case, since the surface temperature in areas with fractional ice cover is also warmer by about 6°C to 16°C , so that the vertical gradient remains or even increases. Secondly, the wind speed in the sensitivity runs is increased over the polynya and thus enhances the turbulent fluxes. The increased sensible heat flux causes also TKE production by buoyancy.

All simulations show a cloud fraction of 0.2—0.4 in the lowest 200 m over the fast ice upstream of the polynya. Almost all sensitivity simulations show considerably less cloud-formation above and downstream the polynya compared to the reference simulation. Although the amount and location of clouds varies, the clouds almost vanish. The reason for this is that the maximum value of the specific humidity is about $0.4 \times 10^{-3} \text{ kg/kg}$ over the AL polynya in all simulations and if the CBL warms, the condensation of water vapour is inhibited. As a result, nearly no clouds form above the polynya. In C05nt and C05wt10 (Fig.

5.1.4 Total atmospheric energy flux

The above mentioned findings result in an increased heat loss from the ocean, which is confirmed and shown in Fig. 8a, d) the cloud fraction over the polynya increases to 0.6 in a layer between about 100—300 m. With thinner ice. In the reference simulation the total atmospheric heat flux (Q_A) is, almost homogeneously, about -500 W m^{-2} over the AL polynya (note that the negative sign denotes upward fluxes). By assuming subgrid-scale sea ice, the cloud fraction in the lower 200 m is less than 0.2 (Fig.8b-e). C05-50/5 and open-water the heat loss considerably increases, exceeding -1000 W m^{-2} at the windward edge and in the center of the polynya. Higher and more structured values of Q_A resulted also from C05-50/01 (Fig. 8e-f) simulates no cloud-formation above and downstream the polynya at all. The increased warming of the boundary layer over the polynya by the sensible heat flux divergence has a larger effect on the relative humidity than the increased moisture input by the latent heat flux. Thus the cloud-formation in the model simulation is reduced for thin subgrid-scale sea ice. The smooth transition at the polynya margins is also visible from this figure. Since we based the estimation of ice production on this quantity it is clear that there will be considerable differences as well.

5.2 Energy balance components for the winter period 2007/08

In order to this section we analyse how the assumptions on subgrid-scale thin ice within the tile-approach affects the energy balance at the surface over the whole winter season 2007/08, we compare 08. We compared daily means of the components of total atmospheric heat fluxes, which were spatially averaged over polynyas (Fig. 97). Thereby, at least 9 grid boxes within the polynya masks have to have had a SIC $\leq 70\%$ in order to be considered in the analysis.

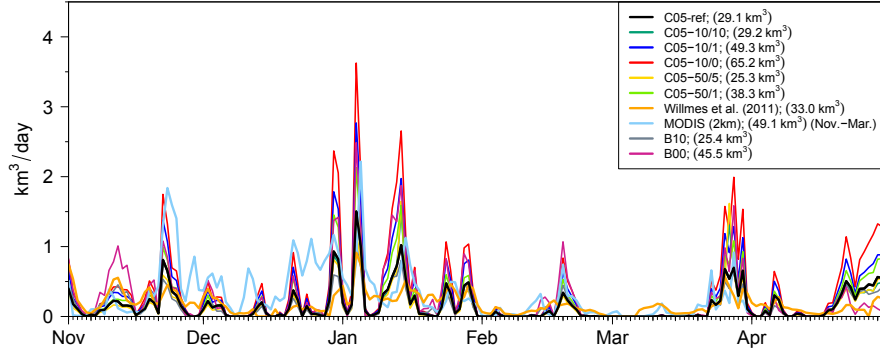


Figure 9. Daily sea-ice production within the Laptev Sea polynyas in the winter period 2007/08, aggregated within the four polynya masks (only considering polynyas $> 277 \text{ km}^2$ in the C05 and [Bauer et al. \(2013\)](#) simulations (B10, B00)). The total sea-ice production is given in parenthesis in the legend (see also Tab. 4).

Table 4. Total sea-ice production (IP) (km^3) in the winter period 2007/08, aggregated over polynyas within the four polynya masks (Fig. 2). The daily mean (\bar{x}) and standard deviation (σ) are given in km^3/day . The Pearson correlation coefficient (r) and the 95% confidence interval (CI) was calculated based on the Fisher z-transformation with the IP time series and the estimates of [Willmes et al. \(2011\)](#). The critical value is $r_{c, \alpha=0.05, n=182} = 0.15$ and r is significant if $r > r_c$. Two-sided t-tests ($\alpha = 5\%$) were performed and the resulting p-values (p) values are given. Significant differences are marked with *. The results from [Bauer et al. \(2013\)](#) assumed an ice thickness of 10 cm (B10) or open-water (B00) within polynyas, both without a tile-approach.

Data	total	\bar{x}	σ	r [95% CI]	p
C05-ref	29.1	0.2	0.2	0.65 [0.56;0.73]	0.30
C05-10/10	29.2	0.2	0.3	0.63 [0.53;0.71]	0.34
C05-10/1	49.3	0.3	0.4	0.63 [0.53;0.71]	0.01*
C05-10/0	65.2	0.4	0.6	0.61 [0.51;0.69]	$< 0.01^*$
C05-50/5	25.3	0.1	0.3	0.56 [0.45;0.65]	0.05*
C05-50/1	38.3	0.2	0.3	0.60 [0.50;0.69]	0.30
Willmes et al.	33.0	0.2	0.2	-	-
MODIS2km ¹	49.1 ¹	0.3 ¹	0.4 ¹	0.45 [0.33;0.56] ²	$< 0.01^*$ ²
B10	25.4	0.1	0.2	0.67 [0.58;0.74]	0.02*
B00	45.5	0.3	0.4	0.68 [0.59;0.75]	0.03*

¹ Only for November - March.

² Comparisons with [Willmes et al. \(2011\)](#) were made only for November - March.

In principle, the processes presented in [section 5.1](#) come into effect whenever a polynya is present. Thus, if the tile-approach is used Q_A is always more negative due to the consideration of subgrid-scale energy fluxes (Fig. 9a7) and more energy or heat is lost from the ocean.

15 ~~Tab.4 summarizes the temporal and spatial means and the deviations (in %) of the energy balance and its components. In C05nt the temporal mean of Q_A is -252.5 W m^{-2} . Two out of the five sensitivity runs simulate less total heat loss with -246.3 W m^{-2} or -2.5% (C05wt10) and -187.7 W m^{-2} or -25.9% (C05-50/5). Considerably higher heat loss is simulated by the runs with~~ In the reference simulation (C05-ref) about -253 W m^{-2} are lost on average within polynyas. If the subgrid-scale open-water or thin-ice between 1–5 cm: -529.0 W m^{-2} or $+109.7\%$ (C05wt0), -414.4 W m^{-2} or $+64.1\%$ (C05wt1), and -303.2 W m^{-2} or $+20.1\%$ is reduced or replaced by open-water, than Q_A is much higher, reaching about -529 W m^{-2} in the latter, which is about $+110\%$. In the simulation with a realistic configuration (C05-50/1) the increase is about $+20\%$ reaching about -303 W m^{-2} on average.

5 The largest contribution to Q_A constitutes the sensible heat flux H (Fig. 9b): ~~7). About 66% in C05nt and slightly less in the sensitivity runs with 57.4% to 65.6%. The highest of the heat is lost via H in the reference simulation, which slightly decreases to 57% to 65.6%, if the tile-approach is used. The strongest~~ impact on the sensible heat flux shows C05wt0, C05-10/0. Here, H doubles from 166.7 W m^{-2} in C05nt to -324.8 W m^{-2} 167 W m^{-2} in C05-ref to -325 W m^{-2} due to the absence of the isolating sea-ice cover. The increase is lower for C05wt1 ($+60.4\%$) and C05-50/1 ($+7.1\%$). For C05wt10 and less in the other
 10 sensitivity simulations, e.g. $+7.1\%$ in case of C05-50/5 the sensible heat flux even reduces by -3.1% and -35.4% . 1.

The other components contribute much less to the heat loss. However, the partitioning changes when subgrid-scale open-water or subgrid-scale thin-ice $< 10 \text{ cm}$ is assumed. Then the contribution of L^* ~~reduces up to -10% , except for C05wt10 and C05-50/5, but~~ the latent heat flux (E) increases by up to $+10\%$, while the net longwave radiation L^* is reduced by up to -10% . The reason for this is on one hand the increase of the vertical gradient of specific humidity (~~Tab.4~~) and on the other hand
 15 the increase of the near-surface wind speed and TKE, enhancing the turbulence above the polynyas. The Bowen ratio reduces accordingly from ~~4.1 (C05nt and C05wt10) to 2.9 (C05wt1), about 4.0 (C05-ref) to 2.3 (C05wt0), 3.1 (C05-50 C05-10/5), 0)~~ and 2.5 (C05-50/1), respectively. Shortwave radiation K^* only becomes ~~of importance~~ important in the time from March until April, when the melting season begins. Therefore, K^* is small compared to the other terms.

6 Effects on sea-ice production

The daily sea-ice production rates were calculated for the individual polynyas as described in [section 3.1](#). Here we ~~compare~~ compared the ice production of ~~CCLM the C05 simulations~~ to the remote sensing estimations of Willmes et al. (2011), to estimates based on MODIS2km ([section 3.1](#)), and to model results of Bauer et al. (2013).

5 6.1 Polynya area

In Fig. ~~10-8~~ daily polynya areas for the winter period 2007/08 are shown. According to the AMSR-E data set, which has been used to prescribe the SIC in CCLM and in the COSMO simulations of Bauer et al. (2013), large polynya events ($> 10^4 \text{ km}^2$)

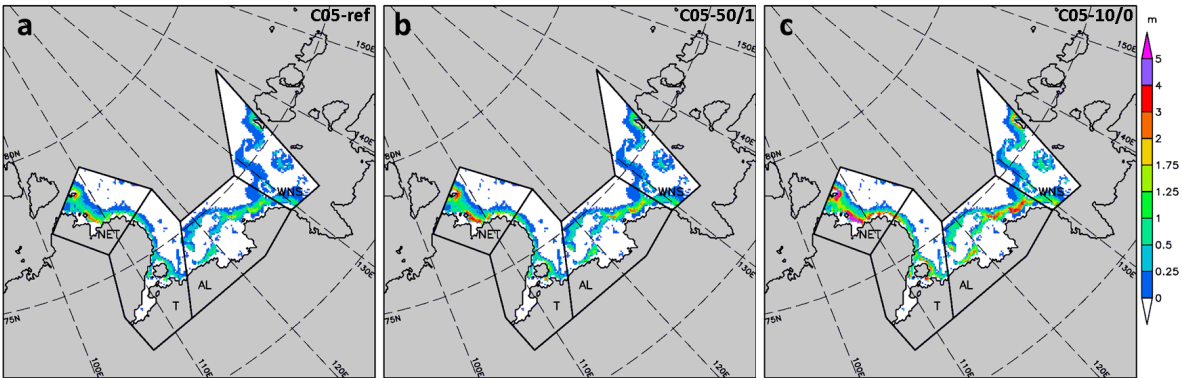


Figure 10. Total sea-ice production (m) within the Laptev Sea polynyas in the winter period 2007/08 simulated by (a) C05-ref (reference), (b) C05-50/1 (realistic), and (c) C05-10/0 (open-water).

occurred at the end of November, in January, and at the end of March. The largest opening event was observed at the end of April. This specific event was object of research in some recent studies, and in March/April. The polynya areas of Willmes et al. (2011) are approximately of the same order as those used for CCLM, whereas the retrieved polynya areas from MODIS2km are considerably higher/larger. This discrepancy is caused by different threshold definitions for polynyas and by different horizontal resolutions. For the MODIS2km data, a polynya is polynyas were defined as areas with thin-ice ≤ 20 cm, as in Preußer et al. (2015b). Given that and the higher horizontal resolution it is likely that also leads within the polynya masks, not resolved by the microwave satellite data, are contributing to the total thin-ice area and hence larger areas result. If areas of open-water outside polynyas are considered as well, then the potential area for ice production increases in CCLM up to the area derived from MODIS2km data, except in the period of late November to the mid of January.

Data total \bar{x} σ r_p C05nt 29.06 0.16 0.24 0.65 0.56;0.730.30C05wt10 29.16 0.16 0.26 0.63 0.53;0.710.34C05wt1 49.31 0.27 0.42 0.63 0.53;0.710.01*C05wt0 65.23 0.36 0.57 0.61 0.51;0.69<0.01*C05-50/525.27 0.14 0.25 0.56 0.45;0.650.05* C05-50/138.27 0.21 0.34 0.60 0.50;0.690.30 Willmes et al. 33.02 0.18 0.16 -- MODIS2km 49.100.320.380.45 0.33;0.56<0.01*B10 25.44 0.14 0.19 0.67 0.58;0.740.02* B00 45.52 0.25 0.40 0.68 0.59;0.750.03*

, which remains lower. Another difference between the polynya area derived from CCLM and in particular the area from Willmes et al. (2011) is that the latter nearly never drops to zero during this winter.

6.2 Ice production in the winter period 2007/08

The time-series of daily IP (km^3/day) are shown in Fig. 11-9 and the total sums ice production for the whole winter are shown in Tab. 22-4. The total IP in the winter 2007/08 is about 29.1 km^3 in the reference simulation (C05nt) is about 29.06 km^3 and only slightly higher in C05wt10 with 29.16 km^3 (+0.3%). Both IP estimates are C05-ref, which is not significantly different to the estimate of from the 33.0 km^3 estimated by Willmes et al. (2011). The temporal correlation is $r = 0.65$, which is sufficiently

high, but some differences are visible (Fig. 9). This result agrees well with the remote sensing estimates, although Willmes et al. (2011) used a constant C_H for calculating the heat fluxes and much coarser atmospheric data.

30 The strongest, significant increase ($p < 0.01$) in IP was simulated by C05wt0 estimated from C05-10/0 with 65.2 km^3 (+125%), where subgrid-scale open-water was assumed. The IP becomes 65.23 km^3 , which constitutes a relative increase of +124.5%. A significant higher IP was also simulated by C05wt1 with 49.31 km^3 (+69.7). A higher IP than in the reference run, but not significantly different from was produced by C05-50/1 with 38.27 km^3 (+38.7) the IP increases to 38.3 km^3 (+39%), which is not significant at the 95%. The only sensitivity run that produced less ice than the reference run is C05-50% level. The increase of IP is caused by the higher heat fluxes from the ocean into the overlying atmosphere as presented above. Compared to the results based on MODIS2km, where we estimated about 49.1 km^3 due to the large polynya area, most of the simulations produced much less ice. Exceptions are C05-10/5 and C05-10/1, which reach or even exceed this estimate. These results show that there are large differences not only between the models but also between remote sensing approaches. For instance, also the time of polynya openings and IP differ ($r = 0.45$). Although such high IP could be reproduced in the Laptev Sea, the question remains which remote sensing data set should be used for calibrating the models.

The IP based on an older reference COSMO simulation by Bauer et al. (2013) with 25.27 km^3 (-13.01%). Comparing the IP of our CCLM simulations with those of, we found a similar ice production of C05-50/5 and B10, which are both lower than cm ice within polynyas (B10) is slightly less compared to our reference run (C05-ref), but significantly lower compared to Willmes et al. (2011). The differences of B10 with respect to C05nt-C05-ref can be explained by differences in the model version, configuration, and nesting chain (GME vs. ERA-Interim, different model domains). The IP of B00 is similar to C05wt1, and thus significantly higher than in-. Of the same order is the IP derived from MODIS2km. The larger polynya areas result in a high ice production of 49.10 km^3 (only Nov.-Mar.), which is significantly different ($p < 0.01$) from the estimated 33.02 km^3 of-.

In general, all model Although the open-water sensitivity run of Bauer et al. (2013) (B00) produces higher IP, it is considerably less compared to our C05-10/0 run. All sensitivity simulations show a higher daily standard deviation than the estimates of compared to the data from Willmes et al. (2011). The temporal correlation of IP based on CCLM and the IP of is $r \approx 0.6$, which increases with decreasing subgrid-scale thin-ice. This is logical since if a polynya opens more heat is released compared to the reference simulation and thus the IP is higher.

Spatial maps of the total IP within polynyas in the winter 2007/08 are shown in Fig. 12. In all simulations the highest IP occurs in the NET polynyas, with rates $> 2 \text{ m}$ in C05nt (Fig. 12a) /winter in C05-ref and $> 5 \text{ m}$ in C05wt0 (/winter in C05-10/0. Further, with considering the subgrid-scale thin-ice or open-water the spatial gradient of ice production is much better represented, with higher rates at the windward edge of the polynyas. Overall, we think that the assumptions made in C05-50/1 are realistic. Although we are aware that open-water areas may occur at the windward site of polynyas, the area of open-water is much smaller compared to the entire polynya area (see Fig. 12e). The lowest IP were simulated in the WNS polynyas. While the results of C05wt10 (Fig. 12d) show no distinct differences with respect to C05nt and C05-50). Thus, the heat flux and IP would be overestimated if open-water is assumed in every grid box with fractional sea ice.

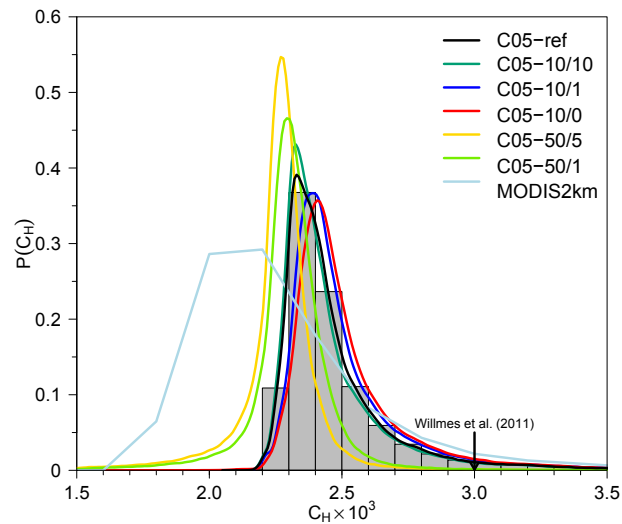


Figure 11. Probability density functions of the turbulent transfer coefficients for heat (C_H) within the Laptev Sea polynyas in the winter period (Nov.-Apr.) 2007/08, aggregated within the four polynya masks. The grey bars show the histogram of C_H from C05-ref. Only values below $6 \cdot 10^{-3}$ have been used for the construction of this figure. The mean values of the C05 simulations are $\approx 2.5 \cdot 10^{-3}$ and the standard deviations are $\approx 0.28 \cdot 10^{-3}$, except for C05-50/5 and C05-50/1 where the mean values are $\approx 2.27 \cdot 10^{-3}$ and $\approx 2.31 \cdot 10^{-3}$, and the standard deviations are $\approx 0.18 \cdot 10^{-3}$, respectively. The constant value of $C_H = 3.0 \cdot 10^{-3}$ of Willmes et al. (2011) is marked with an arrow. The mean C_H value derived from MODIS2km (Nov-Mar.) is $C_H = 2.3 \pm 0.3 \cdot 10^{-3}$.

7 Discussion

The simulation results of our study showed that there is a high sensitivity of the ice production to the assumptions on subgrid-scale thin-ice distribution. Here, a clear relationship was found where the ice production/5 (Fig.12e), heat loss is directly proportional to the thin-ice thickness. This is not surprising but the impact on the ABL showed that the warming of the boundary layer by up to $+3^\circ\text{C}$ did not prevent more heat release due to a weakened vertical temperature gradient. The simulations showed de facto that the vertical gradients remain or even exceed the gradients of the reference simulations. Two effects are responsible for this: (i) as the ice becomes thinner the surface temperature increases stronger than the heating of the ABL, which increases the vertical gradient, and (ii) the near-surface wind speed is enhanced, which increases the wind-shear and thus the sensible heat fluxes. Further, the warm plumes over the polynyas are efficiently advected over the pack ice. Thus heat is removed from above the polynyas and a strong temperature gradient is maintained, which enhances the ice production.

Constraining the assumptions on subgrid-scale thin-ice was found to be difficult. The comparison of model-based IP with remote sensing estimates revealed large discrepancies. Further, large differences were found between the two remote sensing approaches. The usage of higher resolved MODIS data and ERA-Interim, compared to the approach of Willmes et al. (2011),

30 where NCEP and AMSR-E data were used, nearly produced +50% more ice. The configuration of C05-50/1 (Fig. 12f), C05wt1 (Fig. 12e), cm thick grid-scale and C05wt0 (Fig. 12b) produce systematically higher IP, in particular in the AL and NET polynyascm subgrid-scale thin-ice, seems to be a realistic assumption in the marginal ice zone of the polynyas.

The resulting IP is close to the estimates of Willmes et al. (2011), which we defined as a baseline for our sensitivity experiment. However, if for instance the results of MODIS2km would be defined as a baseline, then even thinner ice might
5 be considered. We are aware that our sea-ice module is simplified compared to more sophisticated sea-ice models, where the thin-ice thickness might be a prognostic variable and not a constant. However, despite our simple assumption, the results are promising and satisfactory in order to represent sea ice in a regional climate model in a computationally cheap approach. We further argue, based on our results, that assuming subgrid-scale open-water within fractional sea ice, such as in Polar-WRF (Bromwich et al., 2009) leads to too high heat fluxes from the ocean into the atmosphere.

10 **8 Discussion**

~~Although it~~ However, even if more sophisticated sea-ice models were used to estimate the IP, the issues of how to constrain parameters and to which data set to compare with remain. It is not our intention to entangle all factors controlling the estimation of sea-ice production, we attempted to compile a list of influence factors, which might explain the differences we found while comparing model results with remote sensing results: based on different approaches, data sets or models, but several issues are
15 important in a general sense:

- Polynya area is affected by the definition of polynyas (e.g. $SIC \leq 70\%$ or $h_i < 0.2\text{m}$) and the horizontal resolution of the model and the satellite products.
- Heat loss is affected by ~~differences in the surface temperature, the~~ vertical temperature gradient, wind speed, parameterization of the energy balance components (turbulent fluxes), sea-ice thickness and properties, and by the parameterization of the heat flux through the ice, ~~and by the parameterization of atmospheric turbulent fluxes~~. Particularly important is
20 the horizontal resolution of the atmospheric data set and the assumptions on the turbulent exchange coefficient for heat (C_H). Willmes et al. (2011) assumed a constant value of $C_H = 3 \cdot 10^{-3}$, ~~–~~. However, the mean values from C05 over polynyas (winter 2007/08) are about $(2.5 \pm 0.28) \cdot 10^{-3}$ (Fig. ~~??~~ Except 11), except for C05-50/5 and C05-50/1, which simulated slightly lower values of $(2.27 \pm 0.18) \cdot 10^{-3}$ and $(2.31 \pm 0.18) \cdot 10^{-3}$.
- Since the warm surface temperatures of polynyas and the resulting vertical temperature gradients are not well represented in ERA-Interim or NCEP, the usage of a high value of C_H seems to partly compensate for this issue. The C_H values based on MODIS data and ERA-Interim are lower than simulated by CCLM with a mean of $C_H = (2.3 \pm 0.3) \cdot 10^{-3}$. A similar PDF-probability distribution function was derived by Adams et al. (2013), who combined MODIS and NCEP. Because of the horizontal resolution of MODIS, polynyas are represented as anomalies in the surface temperature causing a field
30 causing larger vertical temperature gradient-gradients and hence C_H values, which are comparable to CCLM.

- Surface temperatures in remote sensing approaches also depend on the number of swaths per day, e.g. clear-sky conditions, and their distribution over the day. If not equally distributed, the surface temperature and the ice production may be biased.

These influence factors together control the sea-ice production estimates and differences between model results and remote sensing. The polynya area is an obvious factor with the simple relationship: the larger the polynya area the larger the sea-ice production. In contrast, the explanations of for differences in the loss of heat or energy loss within polynyas is manifold. In our opinion, the most relevant factors, besides polynya area, are the thin-ice thickness and the parameterizations of the turbulent heat fluxes, in particular the differences in C_H .

5 The complexity of these factors makes make a comparison of model and remote sensing studies difficult. It further indicates that some assumption assumptions in the remote sensing approaches, such as a constant value for C_H , might be oversimplified. Furthermore, a problematic issue is the use usage of coarse atmospheric data sets, such as NCEP or ERA-Interim, for remote sensing approaches, if not combined with high-resolution satellite products. The horizontal resolution of such atmospheric reanalysis data sets is not sufficient to represent polynyas adequately. Thus subsequent errors, such as wrong simulations of
10 the atmospheric boundary layer over polynyas, are the consequence. These errors are then transferred to the remote sensing approach and might result in wrong sea-ice production estimates. From a modelling point of view the question arises what reference for IP estimates should be used? This question is not easily answered and is still an open issue. A strategy might be a simultaneous application of both, modelling and remote sensing approaches, in order to compensate for weaknesses. This issue directly impedes the decision of an optimal model configuration.

15 According to our study, the approach of [Willmes et al. \(2011\)](#) constitutes the closest reference because of the same satellite data that were used to derive polynya area at a comparable horizontal resolution. Although the definition definitions of polynyas are different, the assumption of 0.1 m thin-ice in areas of $SIC \leq 70\%$ is similar to the definition of ≤ 0.2 m as in [Willmes et al. \(2011\)](#). Larger differences evolve from the assumption assumptions made on C_H (Fig. ??11) and the horizontal resolution of the atmospheric data. Given these deviations, the IP based on C05nt, C05wt10, C05-ref and C05-50/1 are still close to the results of [Willmes et al. \(2011\)](#). Although the use of MODIS, i.e. higher resolved satellite products, results in higher IP
5 estimates, the reason for this is the higher horizontal resolution that causes larger polynya areas and not the representation of subgrid-scale energy fluxes within polynyas in ERA-Interim, which is still too coarse. For thicker ice the C_H values converge to $\leq 1.5 \cdot 10^{-3}$, a value also reported by [Schröder et al. \(2003\)](#).

Given these issues, the decision which TIT should be used with the TA is another degree of freedom and cannot sufficiently be answered from our study. A justified assumption is to rely on MODIS TIT (Fig. ??12). The mean derived TIT for the
10 winter periods (Nov.-Mar.) 2002/03–2014/15 is 13.5 ± 0.5 cm, which is slightly thicker than our assumed TIT in CCLM. Unfortunately, the MODIS TIT show distribution for the polynya areas shows no maximum at a specific ice thickness, which gives no preference for the choice of the sub-grid TIT for the tile approach.

~~Based on the statistical analysis, two simulations remain with a similar IP to : C05wt10 and C05-50/1. Although both simulations were performed with a TA, there are two facts that speak for C05-50/1. First, assuming 50 cm as a grid-scale ice
15 thickness is realistic because this thickness can be detected by passive microwave sensors, whereas 10 cm cannot be detected.~~

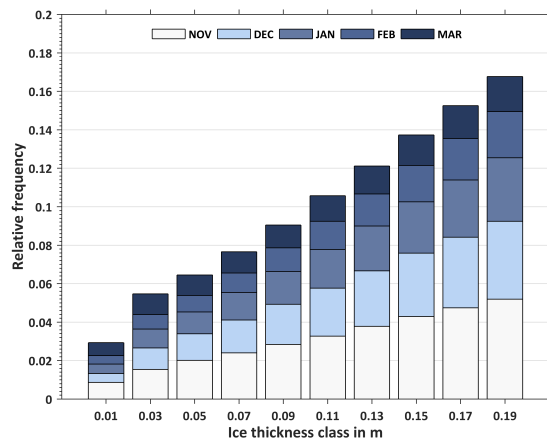


Figure 12. Thin-ice thickness distribution (≤ 20 cm) in the Laptev Sea derived from MODIS data for the winter periods (Nov.-Mar.) 2002/03–2014/15. The bars indicate the relative distribution of each thickness class from the total number of TIT ≤ 0.2 m appearances between the winter seasons 2002/03 and 2014/15. Contributions of each month with respect to the whole winter season for each thickness class are indicated by the blueish colors (see the legend). The mean thickness (\pm one standard deviation) in this period is 13.5 ± 0.5 cm (8.7 cm for ≤ 10 cm). In the winter period 2007/08, the mean is 14.0 ± 2 cm (7.7 cm for ≤ 10 cm).

~~Given that, it is further realistic to assume a subgrid-scale thickness such as 1 cm, which represents the undetectable ice thickness. Second, the estimations with MODIS indicate a higher daily standard deviation compared to , which is similar to σ of C05-50/1.~~

8 Conclusions

20 In this study we ~~implemented a tile approach (TA) for subgrid-scale energy fluxes within fractional sea ice in COSMO-CLM and analysed the sensitivity of sea ice~~ quantified the ice production (IP) of in the Laptev Sea polynyas and the effects for the winter 2007/08 based on CCLM simulations and remote sensing data. A new tile approach (TA) for fractional sea ice, considering subgrid-scale thin-ice, was implemented into CCLM. Besides a reference run, five sensitivity simulations with different assumptions on grid-scale and subgrid-scale ice within polynyas were performed. We further investigated the impact
 25 on the atmospheric boundary layer (ABL) above polynyas.

The results show that the IP is highly sensitive to the assumptions ~~of made on the~~ ice thickness within polynyas associated with the TA.

~~The IP within polynyas increased significantly for most simulations if the . Compared to the estimated IP of 29.1 km^3 of the reference simulation, the IP more than doubled if~~ subgrid-scale ice is thinner than the grid-scale ice. The relative increases
 30 were found to range from $+0.3\%$ to $+124.5\%$ due to a stronger heat loss of up to $+109.7\%$ within polynyas.

open-water was assumed, and increased by about (+39%) for realistic assumptions. The increase of the IP is caused by a larger heat loss from the ocean, whose magnitude is proportional to the thin-ice thickness. Although the ABL is heated by up to +3°C in the open-water configuration, strong vertical temperature gradients and associated high sensible heat fluxes at the surface were maintained. On one side, the TA improves the physical representation of polynyas in CCLM because fractional sea ice is considered, on the other side a new degree of freedom is introduced ~~as it is unclear which ice thickness should be assumed within polynya to constrain the thin-ice thickness~~. The derivation of an optimal configuration ~~of CCLM was not intended in this study, and is yet a difficult task for CCLM or other regional climate models remains difficult~~ because of sparse
5 observed ice thickness distributions within polynyas.

~~Instead we~~ We used remote sensing data as a baseline to ~~compare the simulated IP with. This comparison remained difficult as well because of differences in the definition of polynyas, in the atmospheric forcing and particularly in the calculation of the turbulent diffusion coefficients. The latter were kept either constant for the remote sensing estimations or were calculated from coarse atmospheric data sets, which do not contain polynyas. In CCLM the coefficients were calculated anew every time step with considering polynyas. A next step towards an improved estimation of IP estimations from remote sensing methods could be the use of CCLM data instead of coarse reanalyses. However, showed that this could also lead to problems for MODIS-based methods because of inconsistencies between the CCLM ice distributions and MODIS surface temperatures constrain our configuration, but several issues were found, which hamper such comparisons.~~
10

~~Nevertheless, based on statistics C05-50/1, which assumes a ice thickness of 50 cm at grid-scale and 1 cm at subgrid-scale, simulated the closest ice production with respect to . Besides the good agreement, this configuration is preferred because the AMSR-E sensor is able to detect 50 cm thick ice, but not 1 cm thin ice. Thus, with this model configuration we consider In summary, realistic ice production estimates could be retrieved from our simulations. Neglecting subgrid-scale energy fluxes over fractional sea ice based on reasonable assumptions.~~
15

~~This study shows that CCLM with our implemented TA produces realistic results and improves the representation of polynyas in an atmospheric regional climate model. An extension of our TA would be the separate calculation of the momentum flux for ice and ocean. This would further allow the implementation of a form drag parameterization . The form drag likely increases the turbulence over fractional sea ice and hence the turbulent heat loss over polynyas, which might considerably affect the sea-ice production.~~
20

~~In summary, the implementation of a tile approach for subgrid-scale energy fluxes within fractional sea ice is a large step forward to adapt COSMO-CLM for applications in polar regions might considerably underestimate the ice production in coastal polynyas, such as in the Laptev Sea. As a possible consequence, the vertical mixing and thus the formation of cold, dense bottom water at the Arctic shelf areas might be underestimated with considerable effects on the global thermohaline circulation.~~
25

Appendix A: Sea-ice albedo scheme

We implemented a modified Køltzow scheme (Køltzow, 2007) (Fig. 413) to replace the default treatment of sea-ice albedo, which was previously set to $\alpha_i = 0.75$ for ice thickness > 0.1 m and $\alpha_i = 0.2$ for ice thickness ≤ 0.1 m (Schröder et al., 2011).

Furthermore, the K \ddot{o} ltzow scheme includes a parameterization of melt ponds (see K \ddot{o} ltzow (2007) for details), yet they are of no importance for our study. The scheme is based on measurements retrieved during the Surface heat Budget of the Arctic Ocean (SHEBA) project (Uttal et al., 2002). It is forced by the surface temperature T_{sfc} , which may be either the ice (T_i) or the snow surface temperature (T_s) (Fig. 3). If no snow cover is present the albedo only depends on the ice thickness. If the ice thickness exceeds the threshold value of $h_c = 0.2$ m, a snow cover on sea ice is assumed in accordance to the sea-ice module. Sea ice thicker than h_c is treated as thick ice and the albedo is estimated by:

$$\alpha_i = \begin{cases} 0.84 & \text{if } T_{sfc} \leq -2^\circ\text{C} \\ 0.84 - 0.145(2 + T_{sfc}) & \text{if } 0^\circ\text{C} > T_{sfc} > -2^\circ\text{C} \\ 0.51 & \text{if } T_{sfc} > 0^\circ\text{C}. \end{cases} \quad (\text{A1})$$

K \ddot{o} ltzow (2007) sets the albedo for cold sea ice to a high value of 0.84, which is supposed to include the effects of snow on sea ice in winter and spring. In the original scheme K \ddot{o} ltzow (2007) set the threshold for thin ice to $h_c = 0.25$ m, but since the values above are only valid for snow covered sea ice, we set $h_c = 0.2$ m to be consistent with the sea-ice module.

For thin-ice, we implemented a linear decrease towards the ocean albedo ($\alpha_o = 0.07$):

$$\alpha_i = \alpha_o + (h_i/h_c) \cdot (\alpha_c - \alpha_o) \quad (\text{A2})$$

As a starting value we use $\alpha_c = 0.57$, the albedo of thick bare sea ice from Persson et al. (2002).

Fig. 4 shows a summary of both cases. If the ice thickness is at least 0.2 m (bold black line) then the albedo is constant ($\alpha_i = 0.84$) for cold, snow covered sea ice. It decreases with increasing surface temperature, if -2°C are exceeded. This temperature denotes a threshold where melting begins and sea ice is changing its albedo characteristics. In addition, if melt ponds occur (black solid line), the albedo is somewhat lower during the melting season. The fraction of melt ponds increases with $T_{sfc} > -2^\circ\text{C}$ to a maximum of 22% (bold green line), an upper limit set by K \ddot{o} ltzow (2007), and the albedo of melt ponds converges to the albedo of sea water (dashed green line). Furthermore, in Fig. 4-13 the thin-ice albedo is exemplified for four ice thicknesses which are not covered with snow and for which a constant albedo is assumed (thin black lines).

If the tile-approach is used, subgrid-scale open water reduces the grid-average albedo accordingly, compared to a complete coverage with sea ice. A comparable, though less pronounced, reduction of albedo occurs if 1 cm ~~thin-ice~~ thin-ice coverage is assumed for subgrid-scale open water.

Appendix B: Implementation of the tile-approach in CCLM

In order to simulate the subgrid-scale energy fluxes over fractional sea ice, it is necessary to differentiate the energy balance and its components over water and ice. Over sea ice (index $k = i$) or ocean (index $k = o$) the total atmospheric heat flux (see Fig. 3) is:

$$Q_{A,k} = K_k^* + L_k^* + H_k + E_k \quad (\text{B1})$$

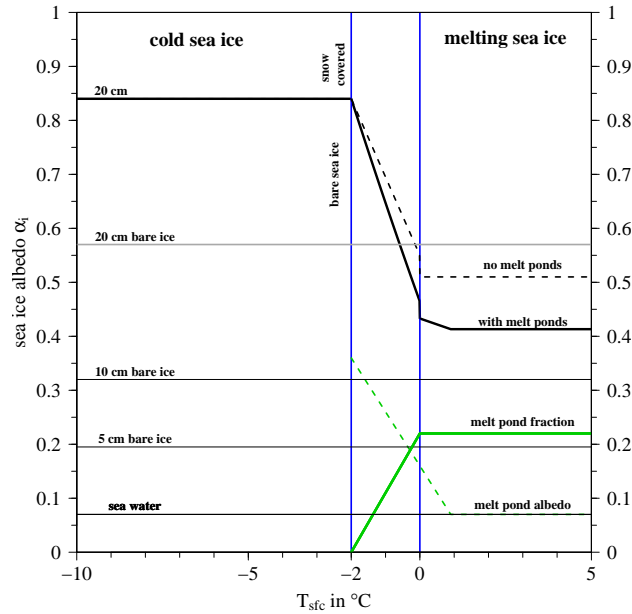


Figure 13. Sea-ice albedo resulting from the modified K \ddot{o} ltzow-scheme (K \ddot{o} ltzow, 2007) in dependence of the ice surface temperature and thickness. Thereby the threshold thickness above which a snow cover of 10 cm is assumed is $h_c = 0.2$ m (bold black line). In addition the melt pond fraction is shown as a function of the ice temperature (bold green line) and the resulting modification (dashed green line) of the sea-ice albedo (dashed black line). For bare sea-ice (thin black lines) a constant albedo value is assumed, which is linearly decreasing from 0.57 (Persson et al., 2002) at 20 cm ice thickness (bold grey line) to 0.07 (ocean albedo, Perovich and Grenfell (1981)), but constant over all surface temperatures, as shown in Eq. (A2). The vertical blue lines mark the transition range from cold to melting conditions.

with K_k^* the net shortwave radiation, L_k^* the net longwave radiation, H_k the turbulent flux of sensible heat and E_k the turbulent flux of latent heat.

All routines of CCLM, except the sea-ice and the turbulence module, calculate with grid-box averaged coefficients or fluxes (flux averaging approach, Vihma (1995)), which is best suited if the sea-ice module only requires the fluxes over ice (L \ddot{u} pkes and Gryanik, 2014). The procedure is described in [section B3](#).

As initial data the module requires the sea surface temperature (SST), the sea-ice fraction (A) and extent, the sea-ice thickness (SIT), the surface temperature of sea ice (T_i), specific humidity at the ice surface, the wind-speed on the lowest model level, and incoming longwave and shortwave radiation (see Schr \ddot{o} der et al. (2011) for more details).

The calculation of the components of the energy balance equations are shown in the next subsections.

B1 Shortwave radiation

- 5 The grid-box average of the albedo α_m (index m for 'mixed') is calculated as:

$$\alpha_m = A \cdot \alpha_i + (1 - A) \cdot \alpha_o, \quad (\text{B2})$$

with A the sea-ice fraction, $\alpha_o = 0.07$ the albedo of the ocean, and $\alpha_i = f(T_i, h)$ the albedo of sea ice as a function of sea ice temperature (T_i) and thickness (h) (see [section A](#)). Based on this mixed albedo the upward shortwave radiation is calculated as:

10 $K \uparrow_m = \alpha_m \cdot K \downarrow,$ (B3)

with $K \downarrow$ the incoming shortwave radiation. The grid-box average net shortwave radiation is calculated as:

$$K_m^* = K \downarrow - K \uparrow_m = (1 - \alpha_m) \cdot K \downarrow. \quad (\text{B4})$$

This grid-box averaged net shortwave radiation is the input for the sea-ice module where the upward shortwave radiation over ice $K \uparrow_i$ is calculated as:

15 $K \uparrow_i = \alpha_i \cdot K \downarrow,$ (B5)

The final net shortwave radiation over sea ice or ocean becomes:

$$K_k^* = (1 - \alpha_k) \cdot K \downarrow = \frac{1 - \alpha_k}{1 - \alpha_m} \cdot K_m^* \quad (\text{B6})$$

where the index k refers either to i (sea ice) or o (ocean).

B2 Longwave radiation

- 20 The subgrid-scale ocean surface temperature (T_o) is assumed to be at the freezing point (-1.7°C) if open water is assumed, or to be a prognostic variable if a thin-ice cover is assumed. The ice surface temperature (T_i) is also a prognostic variable in the sea-ice module.

To account for subgrid-scale longwave radiation, we calculate the upward longwave radiation over sea ice and ocean as:

$$L \uparrow_k = \epsilon \sigma T_k^4 - (1 - \epsilon) L \downarrow, \quad (\text{B7})$$

- 25 with σ the Stefan–Boltzmann constant, $L \downarrow$ the incoming longwave radiation, ϵ the surface emissivities of sea water and ice, which are assumed to be equal ($\epsilon = 0.996$), and T_k the surface temperature of ice or ocean.

Then the net longwave radiation balance over sea ice or ocean becomes:

$$L_k^* = L \downarrow - L \uparrow_k. \quad (\text{B8})$$

B3 Turbulent fluxes of sensible and latent heat

30 We modified the parameterization of the turbulent fluxes of sensible (H) and latent heat (E) within a grid box, in contrast to the standard version of CCLM and the sea-ice module of [Schröder et al. \(2011\)](#). Over sea ice or ocean the roughness length z_0 and the turbulent coefficients of heat and moisture C_H were previously calculated from the predominant surface type of a grid box: ice or sea water. We modified this procedure by a tile-approach; now the fluxes are calculated both for sea ice and ocean within a grid box with different z_0 and C_H . Afterwards they are averaged in a 'flux-averaging approach' and an average C_H is calculated for other modules. The calculation of the momentum flux is not modified and for the details of the calculation we refer the reader to [Doms et al. \(2011\)](#).

In CCLM a stability and roughness length dependent surface flux formulation is used, which is based on flux calculations after [Louis \(1979\)](#). The fluxes are calculated with a bulk approach:

$$H = -\rho c_p C_H |v_h| (\Theta_{sfc} - \Theta) \quad (\text{B9})$$

$$10 \quad E = -\rho L_f C_H |v_h| (q_{sfc} - q) \quad (\text{B10})$$

with ρ the air-density, c_p the heat capacity of air, Θ and Θ_{sfc} the potential temperature at the lowest model layer and at the surface (ice or ocean). q and q_{sfc} are the specific humidity at the lowest model layer and at the surface (ice or ocean), L_f the latent heat of fusion (and sublimation in case of sea ice), $|v_h| = \sqrt{u^2 + v^2}$ the absolute wind speed, and C_H the turbulent transfer coefficient for heat and moisture.

15 To calculate the turbulent transfer coefficients it is first necessary to calculate the roughness length of sea-water ($z_{0,o}$) and sea ice ($z_{0,i}$). In case of sea ice we set $z_{0,i} = 0.001$ m as in [Schröder et al. \(2011\)](#). Over open water a modified Charnock-formula is used (see [Doms et al., 2011](#)). In case of H and E , we assume the additional roughness length for heat z_h ([Doms et al., 2011](#)) to be equal to z_0 over subgrid-scale open ocean within the sea-ice cover.

The transfer coefficients are calculated over sea ice ($C_{H,i}$) and ocean ($C_{H,o}$), respectively. The turbulent fluxes over sea ice 20 (H_i, E_i) and ocean (H_o, E_o) can be retrieved by inserting these coefficients into Eqs. (B9-B10). Then all terms of Eq. (B1) are known to solve the energy balance over both surface types.

The fluxes of sensible and latent heat, the turbulent transfer coefficient for heat, and the surface temperature are averaged according to the sea-ice concentration A :

$$H_m = A \cdot H_i + (1 - A) \cdot H_o \quad (\text{B11})$$

$$5 \quad E_m = A \cdot E_i + (1 - A) \cdot E_o, \quad (\text{B12})$$

$$C_{Hm} = A \cdot C_{H,i} + (1 - A) \cdot C_{H,o}, \quad (\text{B13})$$

$$T_{sfc} = A \cdot T_i + (1 - A) \cdot T_o \quad (\text{B14})$$

The grid averaged temperature fields are used for the comparisons in [section 5](#).

Author contributions. O. Gutjahr implemented the tile-approach and other modifications to the CCLM source code, conducted the CCLM
10 simulations, designed the study and wrote the paper. G. Heinemann assisted in designing the experiments and the structure of the paper, as well as the writing process. A. Preußer wrote the section on MODIS and calculated the sea-ice production from MODIS data, S. Willmes calculated the ice production rates based on AMSR-E and NCEP and assisted in the discussion on the comparison of remote sensing and modelling results. C. Drüe contributed to the translation of the equations into source code.

Acknowledgements. This work was funded by the German Ministry for Education and Research under grant 03G0833D, and is part of the
15 German-Russian Transdrift project. We thank the CLM-Community and the German Weather Service for providing the basic COSMO-CLM model. The AMSR-E data was provided by the University of Bremen, the MODIS data were provided by the US National Snow and Ice Data Center, ERA-Interim by the ECMWF, and the PIOMAS data set by the Polar Science Center (University of Washington). Finally, we thank the DKRZ for providing ~~the computational time.~~ computational time and two anonymous reviewers for critical comments.

References

- 20 Aagard, K., Coachman, L., and Carmack, E.: On the halocline of the Arctic Ocean, *Deep Sea Res.*, 28, 529–545, doi:10.1016/0198-0149(81)90115-1, 1981.
- Adams, S., Willmes, S., Heinemann, G., Rozman, P., Timmermann, R., and Schröder, D.: Evaluation of simulated sea-ice concentrations from sea-ice/ocean models using satellite data and polynya classification methods, *Polar Res.*, 30, doi:10.3402/polar.v30i0.7124, 2011.
- Adams, S., Willmes, S., Schroeder, D., Heinemann, G., Bauer, M., and Krumpfen, T.: Improvement and sensitivity analysis of thermal thin-ice
25 retrievals, *IEEE Trans. Geosci. Remote Sensing*, 51, 3306–3318, 2013.
- Backhaus, J. A., Fohrmann, H., Kaempf, J., and Rubina, A.: Formation and export of water masses produced in Arctic shelf polynyas – Process studies of oceanic convection, *J. Mar. Sci.*, 54, 366–382, 1997.
- Baldauf, M.: A new fast-waves solver for the Runge-Kutta dynamical core, Tech. rep., Deutscher Wetterdienst, 2013.
- Bareiss, J. and Gørgen, K.: Spatial and temporal variability of sea ice in the Laptev Sea: Analyses and review of satellite passive-microwave
30 data and model results, 1979 to 2002, *Global Planet. Change*, 48, 28–54, doi:10.1016/j.gloplacha.2004.12.004, 2005.
- Bauch, D., Schlosser, P., and Fairbanks, R. F.: Freshwater balance and the sources of deep and bottom waters in the Arctic Ocean inferred from the distribution of $H_2^{18}O$, *Prog. Oceanogr.*, 35, 53–80, doi:10.1016/0079-6611(95)00005-2, 1995.
- Bauch, D., Dmitrenko, I. A., Wegner, C., Hölemann, J., Kirillov, S. A., Timokhov, L. A., and Kassens, H.: Exchange of Laptev Sea and Arctic Ocean halocline waters in response to atmospheric forcing, *J. Geophys. Res.*, 114, C05 008, doi:10.1029/2008JC005062, 2009.
- 35 Bauer, M., Schröder, D., Heinemann, G., Willmes, S., and Ebner, L.: Quantifying polynya ice production in the Laptev Sea with the COSMO model, *Polar Res.*, 32, 20922, doi:10.3402/polar.v32i0.20922, 2013.
- Bromwich, D. H., Hines, K. M., and Bai, L.-S.: Development and testing of Polar Weather Research and Forecasting model: 2. Arctic Ocean, *J. Geophys. Res. Atmos.*, 114, D08 122, doi:10.1029/2008JD010300, 2009.
- Dee, D. P., Uppala, S. M., Simmons, A. J., Berrisford, P., Poli, P., Kobayashi, S., Andrae, U., Balmaseda, M. A., Balsamo, G., Bauer, P., Bechtold, P., Beljaars, A. C. M., van de Berg, L., Bidlot, J., Bormann, N., Delsol, C., Dragani, R., Fuentes, M., Geer, A. J., Haimberger, L.,
5 Healy, S. B., Hersbach, H., Hólm, E. V., Isaksen, I., Kåberg, P., Köhler, M., Matricardi, M., McNally, A. P., Monge-Sanz, B. M., Morcrette, J.-J., Park, B.-K., Peubey, C., de Rosnay, P., Tavolato, C., Thépaut, J.-N., and Vitart, F.: The ERA-Interim reanalysis: configuration and performance of the data assimilation system, *Q. J. Roy. Meteor. Soc.*, 137, 553–597, doi:10.1002/qj.828, 2011.
- Dethleff, D., Loewe, P., and Kleine, E.: The Laptev Sea flaw lead – detailed investigation on ice formation and export during 1991/1992 winter season, *Cold. Reg. Sci. Technol.*, 27, 225–243, doi:10.1016/S0165-232X(98)00005-6, 1998.
- 10 Dmitrenko, I., Hölemann, J. A., Tyshko, K., Churun, V., Kirillov, S., and Kassens, H.: The Laptev Sea flaw polynya, Russian Arctic: effects on the mesoscale hydrography, *Ann. Glaciol.*, 33, 373–376, doi:10.3189/172756401781818455, 2001.
- Dmitrenko, I. A., Tyshko, K. N., Kirillov, S. A., Eicken, H., Hölemann, J., and Kassens, H.: Impact of flaw polynyas on the hydrography of the Laptev Sea, *Global Planet. Change*, 48, 9–27, doi:10.1016/j.gloplacha.2004.12.016, 2005.
- Dmitrenko, I. A., Kirillov, S. A., Tremblay, L. B., Bauch, D., and Willmes, S.: Sea-ice production over the Laptev Sea shelf inferred from
15 historical summer-to-winter hydrographic observations of 1960s–1990s, *Geophys. Res. Lett.*, 36, L13 605, doi:10.1029/2009GL038775, 2009.
- Dmitrenko, I. A., Kirillov, S. A., Bloshkina, E., and Lenn, Y.-D.: Tide-induced vertical mixing in the Laptev Sea coastal polynya, *J. Geophys. Res. Oceans*, 117, C00G14, doi:10.1029/2011JC006966, 2012.

- Doms, G., Förster, J., Heise, E., Herzog, H., Raschendorfer, M., Reinhardt, T., Ritter, B., Schrodin, R., Schulz, J.-P., and Vogel, G.: A
20 Description of the Nonhydrostatic Regional COSMO-Model Part II: Physical Parameterization, Consortium for Small-scale Modelling,
Deutscher Wetterdienst, Offenbach, Germany, 2011.
- Ebner, L., Schröder, D., and Heinemann, G.: Impact of Laptev Sea flaw polynyas on the atmospheric boundary layer and ice production using
idealized mesoscale simulations, *Polar Res.*, 30, 7010, doi:10.3402/polar.v30i0.7210, 2011.
- Eicken, H., Dmitrenko, I. A., Tyshko, K., Darovskikh, A., Dierking, W., Blahak, U., Groves, J., and Kassens, H.: Zonation of the Laptev Sea
25 landland ice cover and its importance in a frozen estuary., *Glob. Planet. Change*, 48, 55–83, doi:10.1016/j.gloplacha.2004.12.005, 2005.
- Haid, V., Timmermann, R., Ebner, L., and Heinemann, G.: Atmospheric forcing of coastal polynyas in the south-western Weddell Sea,
Antarct. Sci., pp. 1–15, doi:10.1017/S0954102014000893, 2015.
- Hall, D., Key, J., Casey, K., Riggs, G., and Cavalieri, D.: Sea ice surface temperature product from MODIS, *IEEE Trans. Geosci. Remote
Sens.*, 42, 1076 – 1087, 2004.
- 30 Heinemann, G. and Kerschgens, M.: Comparison of methods for area-averaging surface energy fluxes over heterogeneous land surfaces using
high-resolution non-hydrostatic simulations, *Int. J. Climatol.*, 25, 379–403, doi:10.1002/joc.1123, 2005.
- Heinemann, G. and Rose, L.: Surface energy balance, parameterizations of boundary-layer heights and the application of resistance laws
near an Antarctic Ice Shelf front, *Boundary Layer Meteorol.*, 51, 123–158, doi:10.1007/BF00120464, 1990.
- Heinemann, G., Helbig, A., and Ernsdorf, T.: Russisch–Deutsche Zusammenarbeit: System Laptev-See, Zwischenbericht 2008, *Fahrtbericht
35 der Expedition Transdrift XIII. (Russian–German Cooperation: System Laptev Sea, report 2008, the cruise report of the Transdrift XIII
expedition.)*, chap. Meteorological measurements at the ice edge of the West New Siberian Polynya, pp. 8–19, IFM-GEOMAR, 2009.
- Hines, K. M., Bromwich, D. H., Bai, L., Bitz, C. M., Powers, J. G., and Manning, K. W.: Sea Ice Enhancements to Polar WRF, *Mon. Weather
Rev.*, doi:10.1175/MWR-D-14-00344.1, 2015.
- Ivanov, V. V. and Golovin, P.: Observations and modeling of dense water cascading from the northwestern Laptev Sea, *J. Geophys. Res.*, 112,
C09 003, doi:10.1029/2006JC003882, 2007.
- Iwamoto, K., Ohshima, K. I., and Tamura, T.: Improved mapping of sea ice production in the Arctic Ocean using AMSR-E thin ice
thickness algorithm, *J. Geophys. Res. Oceans*, 119, 3574–3594, doi:10.1002/2013JC009749, [http://onlinelibrary.wiley.com/doi/10.1002/
5 2013JC009749/abstract](http://onlinelibrary.wiley.com/doi/10.1002/2013JC009749/abstract), 2014.
- Køltzow, M.: The effect of a new snow and sea ice albedo scheme on regional climate model simulations, *J. Geophys. Res.*, 112, D07 110,
doi:10.1029/2006JD007693, 2007.
- Krumpen, T., Hölemann, J. A., Willmes, S., Morales Maqueda, M. A., Busche, T., Dmitrenko, I. A., Gerdes, R., Haas, C., Heinemann, G.,
Hendricks, S., Kassens, H., Rabenstein, L., and Schröder, D.: Sea ice production and water mass modification in the eastern Laptev Sea,
10 *J. Geophys. Res.*, 116, C05 014, doi:10.1029/2010JC006545, 2011.
- Krumpen, T., Janout, M., Hodges, K. I., Gerdes, R., Girard-Ardhuin, F., Hölemann, J. A., and Willmes, S.: Variability and trends in Laptev
Sea ice outflow between 1992–2011, *Cryosphere*, 7, 349–363, doi:10.5194/tc-7-349-2013, 2013.
- Launiainen, J. and Vihma, T.: Derivation of turbulent surface fluxes - An iterative flux-profile method allowing arbitrary observing heights,
Environ. Softw., 5, 113–124, doi:10.1016/02669838(90)90021-w, 1990.
- 15 Louis, J.-F.: A parametric model of vertical eddy fluxes in the atmosphere, *Boundary Layer Meteorol.*, 17, 187–202,
doi:10.1007/BF00117978, 1979.
- Lüpkes, C. and Gryanik, V. M.: A stability dependent parametrization of transfer coefficients for momentum and heat over polar sea ice to
be used in climate models, *J. Geophys. Res. Atmos.*, p. 2014JD022418, doi:10.1002/2014JD022418, 2014.

- Markus, T. and Burns, B. A.: A method to estimate subpixel-scale coastal polynyas with satellite passive microwave data, *J. Geophys. Res. Oceans*, 100, 4473–4487, doi:10.1029/94JC02278, 1995.
- 20 Martin, S. and Kauffmann, P.: A field and laboratory study of wave dumping by grease ice, *J. Glacial.*, 27, 293–313, 1981.
- Massom, R. A., Harris, P. T., Michael, K. J., and Potter, M.: The distribution and formative processes of latent-heat polynyas in East Antarctica, *Ann. Glaciol.*, 27, 420–426, 1998.
- Mellor, G. L. and Yamada, T.: A Hierarchy of Turbulence Closure Models for Planetary Boundary Layers, *J. Atmos. Sci.*, 31, 1791–1806, doi:10.1175/1520-0469(1974)031<1791:AHOTCM>2.0.CO;2, 1974.
- 25 Mironov, D., Ritter, B., Schulz, J.-P., Buchhold, M., Lange, M., and Machulskaya, E.: Parameterisation of sea and lake ice in numerical weather prediction models of the German Weather Service, *Tellus A*, 64, 17 330, doi:10.3402/tellusa.v64i0.17330, 2012.
- Morales Maqueda, M. A., Willmott, A. J., and Biggs, N. R. T.: Polynya Dynamics: a Review of Observations and Modeling, *Rev. Geophys.*, 42, RG1004, doi:10.1029/2002RG000116, 2004.
- 30 Paul, S., Willmes, S., Gutjahr, O., Preußner, A., and Heinemann, G.: Spatial Feature Reconstruction of Cloud-Covered Areas in Daily MODIS Composites, *Rem. Sens.*, 7, 5042–5056, doi:10.3390/rs70505042, <http://www.mdpi.com/2072-4292/7/5/5042>, 2015.
- Perovich, D. K. and Grenfell, T. C.: Laboratory studies of the optical properties of young sea ice, *J. Glacial.*, 27, 331–346, 1981.
- Persson, P. O. G., Fairall, C. W., Andreas, E. L., Guest, P., and D., K.: Measurements near the Atmospheric Surface Flux Group tower at SHEBA: Near-surface conditions and surface energy budget, *J. Geophys. Res.*, 107(C10), 8045, doi:10.1029/2000JC000705, 2002.
- 35 Preußner, A., Heinemann, G., and Willmes: Multi-Decadal variability of Thin-Ice Dynamics and Ice Production in the North Water Polynya by means of Passive Microwave and Thermal Infrared Satellite Imagery, *Rem. Sens.*, 7(12), 15 844–15 867, doi:10.3390/rs71215807, 2015a.
- Preußner, A., Willmes, S., Heinemann, G., and Paul, S.: Thin-ice dynamics and ice production in the Storfjorden polynya for winter-seasons 2002/2003–2013/2014 using MODIS thermal infrared imagery, *Cryosphere*, 9, 1063–1073, doi:10.5194/tcd-8-5763-2014, 2015b.
- Riggs, G., Hall, D., and Salomonson, V.: MODIS Sea Ice Products User Guide to Collection 5, NSIDC, 2006.
- Rigor, I. G. and Colony, R. L.: Sea-ice production and transport of pollutants in the Laptev Sea, *Sci. Total Environ.*, 202, 89–110, 1997.
- Ritter, B. and Geleyn, J.-F.: A Comprehensive Radiation Scheme for Numerical Weather Prediction Models with Potential Applications in Climate Simulations, *Mon. Weather Rev.*, 120, 303–325, doi:10.1175/1520-0493(1992)120<0303:ACRSFN>2.0.CO;2, 1992.
- 5 Rockel, B., Will, A., and Hense, A.: The Regional Climate Model COSMO-CLM (CCLM), *Met. Z.*, 17(4), 347–348, 2008.
- Schröder, D., Vihma, T., Kerber, A., and Brümmer, B.: On the parameterization of turbulent surface fluxes over heterogeneous sea ice surfaces, *J. Geophys. Res. Oceans*, 108, 3195, doi:10.1029/2002JC001385, 2003.
- Schröder, D., Heinemann, G., and Willmes, S.: The impact of a thermodynamic sea-ice module in the COSMO numerical weather prediction model on simulations for the Laptev Sea, Siberian Arctic, *Polar Res.*, 30, 6334, doi:10.3402/polar.v30i0.6334, 2011.
- 10 Schweiger, A., Lindsay, R., Zhang, J., Steele, M., Stern, H., and Kwok, R.: Uncertainty in modeled Arctic sea ice volume, *J. Geophys. Res. Oceans*, 116, C00D06, doi:10.1029/2011JC007084, 2011.
- Smedsrud, L. H. and Martin, T.: Grease ice in basin-scale sea-ice ocean models, *Ann. Glaciol.*, 56(69), 295–306, doi:10.3189/2015AoG69A765, 2015.
- 15 Smith, S. D., Muench, R. D., and Pease, C. H.: Polynyas and leads: An overview of physical processes and environment, *J. Geophys. Res. Oceans*, 95, 9461–9479, doi:10.1029/JC095iC06p09461, 1990.
- Spreen, G., Kaleschke, L., and Heygster, G.: Sea ice remote sensing using AMSR-E 89-GHz channels, *J. Geophys. Res. Oceans*, 113, C02S03, doi:10.1029/2005JC003384, 2008.

- Steppeler, J., Doms, G., Schättler, U., Bitzer, H. W., Gassmann, A., Damrath, U., and Gregoric, G.: Meso-gamma scale forecasts using the
20 nonhydrostatic model LM, *Meteor. Atmos. Phys.*, 82, 75–96, doi:10.1007/s00703-001-0592-9, 2003.
- Tamura, T. and Ohshima, K. I.: Mapping of sea ice production in the Arctic coastal polynyas, *J. Geophys. Res. Oceans*, 116, C07 030,
doi:10.1029/2010JC006586, <http://onlinelibrary.wiley.com/doi/10.1029/2010JC006586/abstract>, 2011.
- Timokhov, L. A.: Regional characteristics of the Laptev and the East Siberian seas: climate, topography, ice phases, thermohaline regime,
circulation., *Ber. Polarforsch.*, 114, 15–32, <http://epic.awi.de/26322/1/BerPolarforsch1994144.pdf>, 1994.
- 25 Uttal, T., Curry, J. A., Mcphee, M. G., Perovich, D. K., Moritz, R. E., Maslanik, J. A., Guest, P. S., Stern, H. L., Moore, J. A., Turenne, R.,
Heiberg, A., Serreze, M. C., Wylie, D. P., Persson, O. G., Paulson, C. A., Halle, C., Morison, J. H., Wheeler, P. A., Makshtas, A., Welch,
H., Shupe, M. D., Intrieri, J. M., Stannnes, K., Lindsey, R. W., Pinkel, R., Pegau, W. S., Stanton, T. P., and Grenfeld, T. C.: Surface Heat
855 Budget of the Arctic Ocean, *Bull. Am. Meteorol. Soc.*, 83, 255–275, doi:10.1175/1520-0477(2002)083<0255:SHBOTA>2.3.CO;2, 2002.
- Van Pham, T., Brauch, J., Dieterich, C., Frueh, B., and Ahrens, B.: New coupled atmosphere-ocean-ice system COSMO-CLM/NEMO:
assessing air temperature sensitivity over the North and Baltic Seas, *Oceanologia*, 56, 167–189, doi:10.5697/oc.56-2.167, 2014.
- Vihma, T.: Subgrid parameterization of surface heat and momentum fluxes over polar oceans, *J. Geophys. Res. Oceans*, 100, 22 625–22 646,
doi:10.1029/95JC02498, 1995.
- 860 Wicker, L. J. and Skamarock, W. C.: Time-Splitting Methods for Elastic Models Using Forward Time Schemes, *Mon.
Weather Rev.*, 130, 2088–2097, doi:10.1175/1520-0493(2002)130<2088:TSMFEM>2.0.CO;2, [http://journals.ametsoc.org/doi/abs/10.
1175/1520-0493\(2002\)130%3C2088%3ATSMFEM%3E2.0.CO%3B2](http://journals.ametsoc.org/doi/abs/10.1175/1520-0493(2002)130%3C2088%3ATSMFEM%3E2.0.CO%3B2), 2002.
- Willmes, S., Krumpen, T., Adams, S., Rabenstein, L., and Haas, C.: Cross-validation of polynya monitoring methods from multi-sensor
satellite and airborne data: A case study., *Can. J. Remote Sens.*, pp. 196–210, doi:10.5589/m10-012, 2010.
- 865 Willmes, S., Adams, S., Schröder, D., and Heinemann, G.: Spatio-temporal variability of polynya dynamics and ice production in the Laptev
Sea between the winters of 1979/80 and 2007/08, *Polar Res.*, 30, 5971, doi:10.3402/polar.v30i0.5971, 2011.
- Yu, Y. and Lindsay, R.: Comparison of thin ice thickness distributions derived from RADARSAT Geophysical Processor System and ad-
vanced very high resolution radiometer data sets, *J. Geophys. Res.*, 108, 3387, 2003.
- Yu, Y. and Rothrock, D. A.: Thin ice thickness from satellite thermal imagery, *J. Geophys. Res.*, 101, 25 753–25 766, 1996.
- 870 Zhang, J. and Rothrock, D. A.: Modeling Global Sea Ice with a Thickness and Enthalpy Distribution Model in Generalized Curvilinear
Coordinates, *Mon. Weather Rev.*, 131, 845–861, doi:10.1175/1520-0493(2003)131<0845:MGSIWA>2.0.CO;2, 2003.